IMMUNOLOGY

Reciprocal regulation of mTORC1 signaling and ribosomal biosynthesis determines cell cycle progression in activated T cells

Teresa Rosenlehner¹†‡, Stefanie Pennavaria¹†‡, Batuhan Akçabozan¹, Shiva Jahani¹, Thomas J. O'Neill², Daniel Krappmann², Tobias Straub³, Jan Kranich¹, Reinhard Obst¹*

Ribosomal biosynthesis in nucleoli is an energy-demanding process driven by all RNA polymerases and hundreds of auxiliary proteins. We investigated how this process is regulated in activated T lymphocytes by T cell receptor (TCR) signals and the multiprotein complexes mTORC1 and mTORC2, both of which contain the kinase mTOR. Deficiency in mTORC1 slowed the proliferation of T cells, with further delays in each consecutive division, an effect not seen with deficiency in mTORC2. mTORC1 signaling was stimulated by components of conventional TCR signaling, and, reciprocally, TCR sensitivity was decreased by mTORC1 inhibition. The substantial increase in the amount of RNA per cell induced by TCR activation was reduced by 50% by deficiency in mTORC1, but not in mTORC2 or in S6 kinases 1 and 2, which are activated downstream of mTORC1. RNA-seq data showed that mTORC1 deficiency reduced the abundance of all RNA biotypes, although rRNA processing was largely intact in activated T cells. Imaging cytometry with FISH probes for nascent pre-rRNA revealed that deletion of mTORC1, but not that of mTORC2, reduced the number and expansion of nucleolar sites of active transcription. Protein translation was consequently decreased by 50% in the absence of mTORC1. Inhibiting RNA polymerase I blocked not only proliferation but also mTORC1 signaling. Our data show that TCR signaling, mTORC1 activity, and ribosomal biosynthesis in the nucleolus regulate each other during biomass production in clonally expanding T cells.



Copyright © 2024 True
Authors, some rights
reserved; exclusive
licensee American
Association for the
Advancement of
Science. No claim to
original U.S.
Government Works

INTRODUCTION

T cells have been engineered for new therapies of malignancies. However, many roadblocks remain, and a better understanding of how T cell receptor (TCR)-dependent signaling reprograms cellular physiology for rapid clonal expansion and effector functions may help to inform new cell therapies (1). TCR-mediated antigen recognition drives T cells to quickly adapt their metabolism from dormancy to macromolecular biosynthesis and energy production. During clonal expansion, which is potentially unlimited (2), T cells divide with a rate of about three divisions per day, which is among the fastest in the adult organism. TCR-initiated signaling events have been elucidated by the analysis of activation markers such as interleukin-2 (IL-2), CD69, or nuclear receptor 4a1 (NR4a1) (3-6) and of the shift to anabolic metabolism (7–13). Activated T cells use aerobic glycolysis to funnel glycolytic intermediates to biosynthetic pathways, including nucleotide biosynthesis through the pentose phosphate pathway, while optimizing mitochondrial physiology for adenosine 5'-triphosphate production (8, 14, 15). The exploration of metabolic shifts in T cells holds promise for cancer therapy because transient inhibition of TCR signaling can enhance the functionality of tumor-exhausted T cells (16-25).

The evolutionarily conserved mTOR (mammalian target of rapamycin) complexes (mTORCs) are Ser/Thr kinases that adapt multiple cellular functions to receptor-mediated signals and microenvironmental nutrient availability (11, 26). In activated T cells, the Raptor-containing

mTORC1 is required for the increased activity and maintenance of glucose and amino acid transporters for aerobic glycolysis (27–32), as well as for lysosomal biogenesis and autophagy (33, 34). The Rictor-containing mTORC2 is critical for memory T cell maintenance (35, 36). mTORC1 also affects CD4⁺ T helper 1 (T_H1), T_H2, T_H17, and T memory cell differentiation (29, 37, 38), and the TCR-dependent maintenance and function of regulatory T cells also depend on mTORC1 activity and amino acid transporter induction (39–42). mTORC1 activity is compromised in antigen-, virus-, and tumor-exhausted T cells (43–45), which makes mTORC1 and its downstream effectors a potential target for immunointervention (16, 18, 38, 46, 47).

Protein synthesis is considered a "housekeeping" function but varies on a global level between tissues depending on homeostatic demands. It is dynamically enhanced in activated lymphocytes (48–52). In actively proliferating eukaryotic cells, ribosomal biosynthesis makes up 40 to 80% of cellular transcription by all three RNA polymerases (Pol) and may require ~60% of the cells' energy (53-55). In mammalian cells, Pol I activity determines the capacity of cells to grow and proliferate, which makes the nucleolus the point of convergence integrating the demand of synthesizing millions of ribosomes per cell cycle. In the nucleolus, ribosomal RNA (rRNA) is transcribed from five tandem arrays of hundreds of ribosomal DNA (rDNA) repeats and processed and modified at ~230 sites by ~200 ribosomal biosynthesis proteins and ~80 small nucleolar RNAs. Ribosomal subunits are assembled from four RNAs and 79 ribosomal proteins (54–59). In yeast and tumor cells, these processes are mostly under transcriptional control and regulated by mTORC1 (60).

Here, we explored mTORC signaling and ribosomal biosynthesis in T cells, which are two of the primary targets of rapalogs. We showed that T cell activation increased the amount of RNA per cell at least ninefold, an increase that was halved by the absence of

¹Institute for Immunology, Biomedical Center, Medical Faculty, Ludwig-Maximilians-Universität München, 82152 Planegg-Martinsried, Germany. ²Research Unit Signaling and Translation, Helmholtz Zentrum München, 85764 Neuherberg, Germany. ³Bioinformatics Core Facility, Biomedical Center, Medical Faculty, Ludwig-Maximilians-Universität München, 82152 Planegg-Martinsried, Germany.

^{*}Corresponding author. Email: reinhard.obst@med.uni-muenchen.de

[†]Present address: Bavarian Nordic, 82152 Planegg-Martinsried, Germany.

[‡]These authors contributed equally to this work.

mTORC1. Sequencing of all RNA biotypes indicated that rRNA constituted 85% of a T cell's RNA, independently of activation status, T cell subset, or mTORC1 activity. The abundance of rRNA was mostly controlled by transcription rather than 47S pre-rRNA processing and affected structural features of the nucleolus and the nucleus and delaying increases in cell size. Chemical mTORC1 inhibition decreased rRNA abundance and slowed proliferation, whereas Pol I inhibition attenuated both proliferation and mTORC1 activity, indicating reciprocal regulation of mTORC1 and the nucleolus that supplies the cells' anabolic infrastructure.

RESULTS

T cell proliferation is restricted by the absence of mTORC1, but not that of mTORC2

Because it is unclear how T cell proliferation is compromised by the deletion of mTOR components (32, 61–63), we investigated the role of mTORC1 and mTORC2 in T cell reactivity in vivo. We transferred CellTracker Violet (CTV)-labeled B6-CD45.1⁺ CD4-cre⁺ wildtype (WT), CD4- cre^+ $Raptor^{fl/fl}$ ($Raptor^{CD4}$), or CD4- cre^+ $Rictor^{fl/fl}$ ($Rictor^{CD4}$) T cells into H2- $A^{b/bm12}$ or H2- $K^{b/bm1}$ recipients. Each of these H2 variants carry three amino acid substitutions that affect peptide binding and thus make them strong alloantigens for $H2^{b/b}$ CD4⁺ and CD8⁺ T cells, respectively (64). Western blot analysis confirmed the removal of Raptor and Rictor in mature T cells of the respective genotypes (fig. S1). Although WT and Rictor^{CD4} CD4⁺ T cells responsive to A^{bm12} divided homogeneously six or more times within 5 days, *Raptor*^{CD4} cells divided one to six times over the same period (Fig. 1A). Similarly, Raptor^{CD4} K^{bm1}-reactive CD8⁺ T cells underwent a variable number of divisions (Fig. 1B). These results suggested that each consecutive division of both CD4⁺ and CD8⁺ T cells responding to a constitutively presented antigen in vivo is delayed in the absence of mTORC1, but not by that of mTORC2.

Because polyclonal alloreactive cells have a wide range of TCR affinities, we next asked how T cells with defined specificity responded to constitutively presented antigen in the absence of mTORC1. Congenically marked WT and Raptor AND-TCR transgenic T cells were cotransferred into inducible moth cytochrome c (iMCC) recipients whose dendritic cells and macrophages constitutively present their cognate antigen H2-E^k/MCC₉₃₋₁₀₃ when fed doxycycline (dox) (45). WT cells went through ~3 divisions/day, a rate generally found in response to pathogens as well (65). However, Raptor^{CD4} AND T cells proliferated with the constantly lower rate of 1 or 2 divisions/day and did not accumulate as efficiently as did WT cells (Fig. 1C). Upon transfer into dox-fed iOVA mice, which present the ovalbumin peptide OVA₂₅₇₋₂₆₄ (OVAp) through H2-K^b under dox control (66), Raptor^{CD4} CD8⁺ OT1 T cells showed a similarly reduced rate of division compared to cotransferred WT cells (Fig. 1D). These data confirm that each consecutive division of T cells proliferating in vivo is hampered in the absence of mTORC1. For more detailed analyses, we turned to T cells activated in vitro; how such cells were gated is shown in fig. S2. Raptor^{CD4} CD8⁺ T cells divided at about half the rate of WT cells (Fig. 1E), thus corroborating the in vivo findings. 5-Ethynyl-2'deoxyuridine (EdU) pulse labeling showed that fewer Raptor CD4 T cells entered S phase, indicating that the absence of mTORC1 restricted the G₁-S transition (Fig. 1F, top). Over the following chase periods of 3 and 7 hours, the *Raptor*^{CD4} T cells ran through G_2 and mitosis into the EdU⁺ G₁ gate at a rate that was further reduced, perhaps indicating additional mTORC1-dependent restriction in the S phase or at the

 G_2 -M restriction point (Fig. 1F, middle and bottom), which has been reported in other systems (67). In summary, these data show that T cell proliferation in vivo is three times slower in the absence of mTORC1, which restricts the cell cycle most prominently at the G_1 -S transition (32, 68), whereas the deletion of mTORC2 has no effect.

The relationship between conventional and mTORC1-dependent TCR signaling

mTORC1-dependent signaling integrates multiple environmental cues to adjust T cell metabolism and responses accordingly. Mutual amplification or inhibition of signaling pathways indicates early integration of such cues. We thus asked whether and when TCR- and IL-2-derived signals acted on mTORC1 activity in the course of T cell priming. The phosphorylation of the ribosomal protein S6 (eS6) (56) by the kinases S6 kinase 1 (S6K1) and S6K2 (encoded by the genes *Rps6kb1* and *Rps6kb2*) and the ribosomal protein S6 kinases RSK1 to RSK6 (encoded by Rps6ka1 to Rps6ka6) mostly indicates mTORC1 activity (69, 70), which is detectable within 2 hours of TCR stimulation and is maintained by the TCR for at least 2 days. When TCR stimulation was interrupted, mTORC1 activity decreased (Fig. 2A, left). In contrast, the abundance of IL-2 receptor α (IL-2Rα) chain (CD25) was increased within 2 days and maintained despite TCR signal interruption (Fig. 2A, right). After the rest period of 12 hours, the cells were restimulated with immobilized anti-CD3 antibodies or IL-2 in the absence or presence of tofacitinib, an inhibitor of the IL-2R-associated Janus kinases 1 and 3 (71, 72). Although to facitinib inhibited IL-2-induced mTORC1 activity, it did not interfere with TCR signals (Fig. 2B). These data indicate that TCRand IL-2-dependent signaling pathways can independently trigger mTORC1 kinase activity in activated CD25⁺ T cells (11, 29, 32, 72, 73), likely in a consecutive manner.

CD28-dependent costimulation increased the antigen sensitivity of the TCR 100-fold, as assessed by CD69 abundance (Fig. 2C, left) and mTORC1 activity (Fig. 2B, right), indicating that both conventional and mTORC1-dependent TCR signaling follow the same costimulatory rules. Conventional TCR signaling includes the Ca²⁺/ calcineurin/nuclear factor of activated T cells (NFAT)-, mitogenactivated protein kinase (MAPK)/activating protein 1-, and phosphatidylinositol 3-kinase (PI3K)/Akt-dependent pathways. Inhibitors of each of these pathways (cyclosporin A, GDC0973, and GCD0941, respectively) inhibited CD69 expression (Fig. 2D, top), but mTORC1 activity was not affected by calcineurin and hardly by MAPK inhibition as determined using both S6-pSer^{235/6} – and S6-pSer^{240/4} – specific antibodies (Fig. 2C, bottom, and fig. S2). A possible caveat of these experiments is that S6 phosphorylation is an indirect measure of mTORC1 activity that could also be mediated by other potentially MAPK-dependent kinases (70, 74).

Because the relationship between the nuclear factor κB (NF-κB) and mTORC1 pathways is unclear (75, 76), we tested animals lacking the paracaspase Malt1 (mucosa associated lymphoid tissue lymphoma translocation gene 1), which is required for TCR signal transmission through the caspase recruitment domain family member 11 (Card11)/B cell leukemia/lymphoma 10 (Bcl10)/Malt1 (CBM) complex toward the NF-κB family of transcription factors (77, 78). *Malt1*-deleted cells did not show changes in CD69 abundance (Fig. 2E) but showed decreased S6 phosphorylation (Fig. 2F). These data indicate that conventional and mTORC signaling are controlled to a similar extent by the PI3K/Akt pathway and that the Ca²⁺/calcineurin pathway does not affect mTORC1. Moreover, the

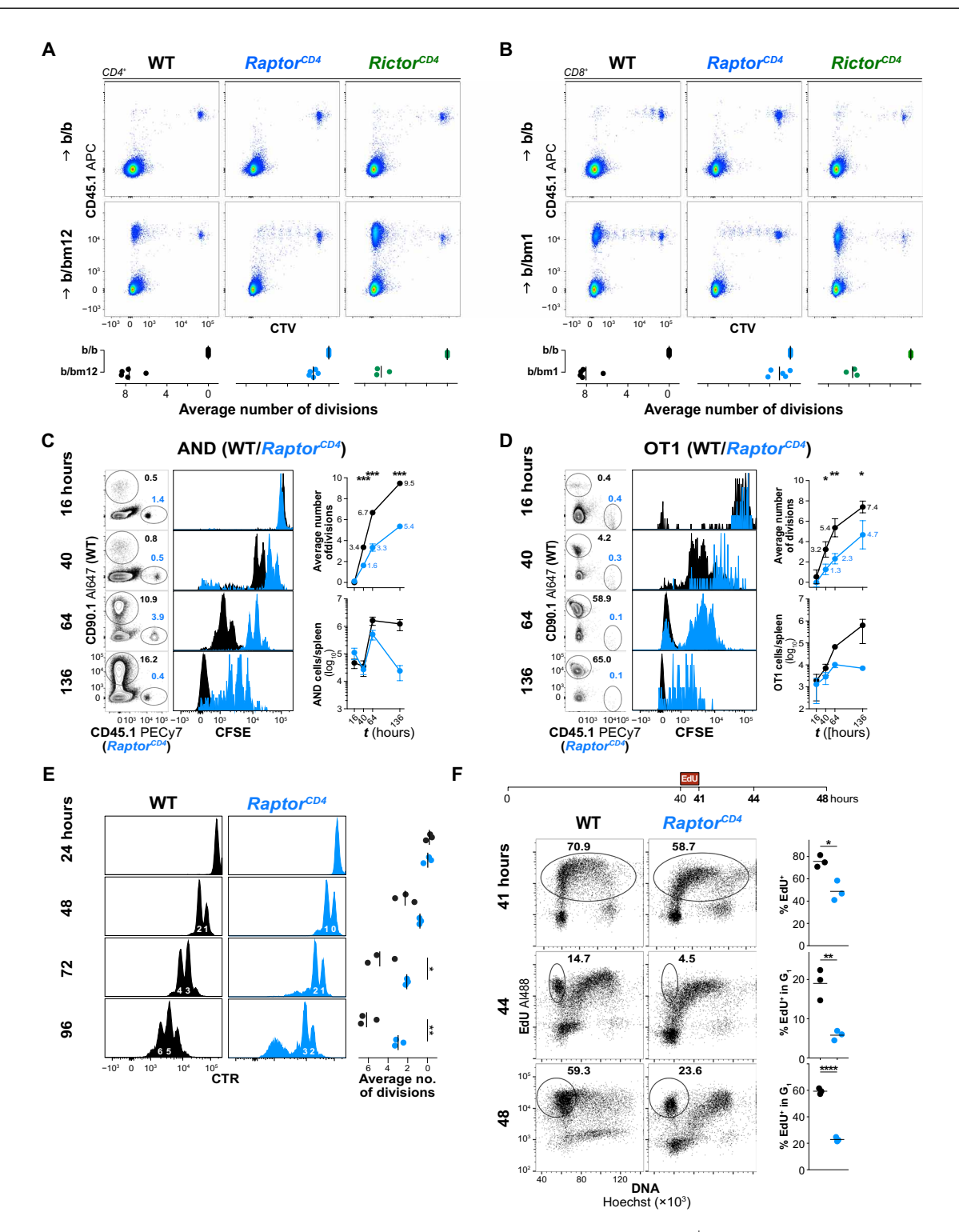


Fig. 1. Control of T cell proliferation by mTORC1 but not by mTORC2. (**A** and **B**) CTV dilution of alloreactive CD45.1 $^+$ WT, *Raptor-*, or *Rictor*-deleted T cells (*Raptor*^{CD4} and *Raptor*^{CD4}, respectively) 5 days after transfer to $H2^{b/b}$ and $H2^{b/bm12}$ (A) or $H2^{b/b}$ and $H2^{b/bm1}$ (B) recipients. CD4 $^+$ (A) and CD8 $^+$ (B) splenocytes from N = 5 (WT and *Raptor*^{CD4}) and N = 3 (*Rictor*^{CD4}) animals were analyzed. (**C**) Proliferation of WT and *Raptor*^{CD4} CD4 $^+$ AND TCR transgenic T cells cotransferred into dox-fed iMCC recipients. Before transfer, the cells were labeled with the CellTracker dye CFSE. Splenocytes from N = 3 animals per genotype were analyzed. (**D**) Proliferation of WT and *Raptor*^{CD4} CD8 $^+$ OT1 TCR transgenic T cells cotransferred into dox-fed iOVA recipients. Splenocytes from N = 3 animals per genotype were analyzed. (**E**) Comparison of OT1 WT and *Raptor*^{CD4} T cell proliferation in response to OVAp (10 ng/ml) over time. CD8 $^+$ T cells labeled with the CTR dye from N = 3 animals per genotype were analyzed. (**F**) In vitro activated OT1 WT or *Raptor*^{CD4}T cells were pulsed with EdU for 1 hour, and EdU incorporation was measured directly after the pulse (top), 3 hours (middle), and 7 hours (bottom) later. CD8 $^+$ T cells from N = 3 animals per genotype were analyzed. *P < 0.05, **P < 0.01, ***P < 0.001, and ****P < 0.0001 by unpaired two-tailed Student's t test.

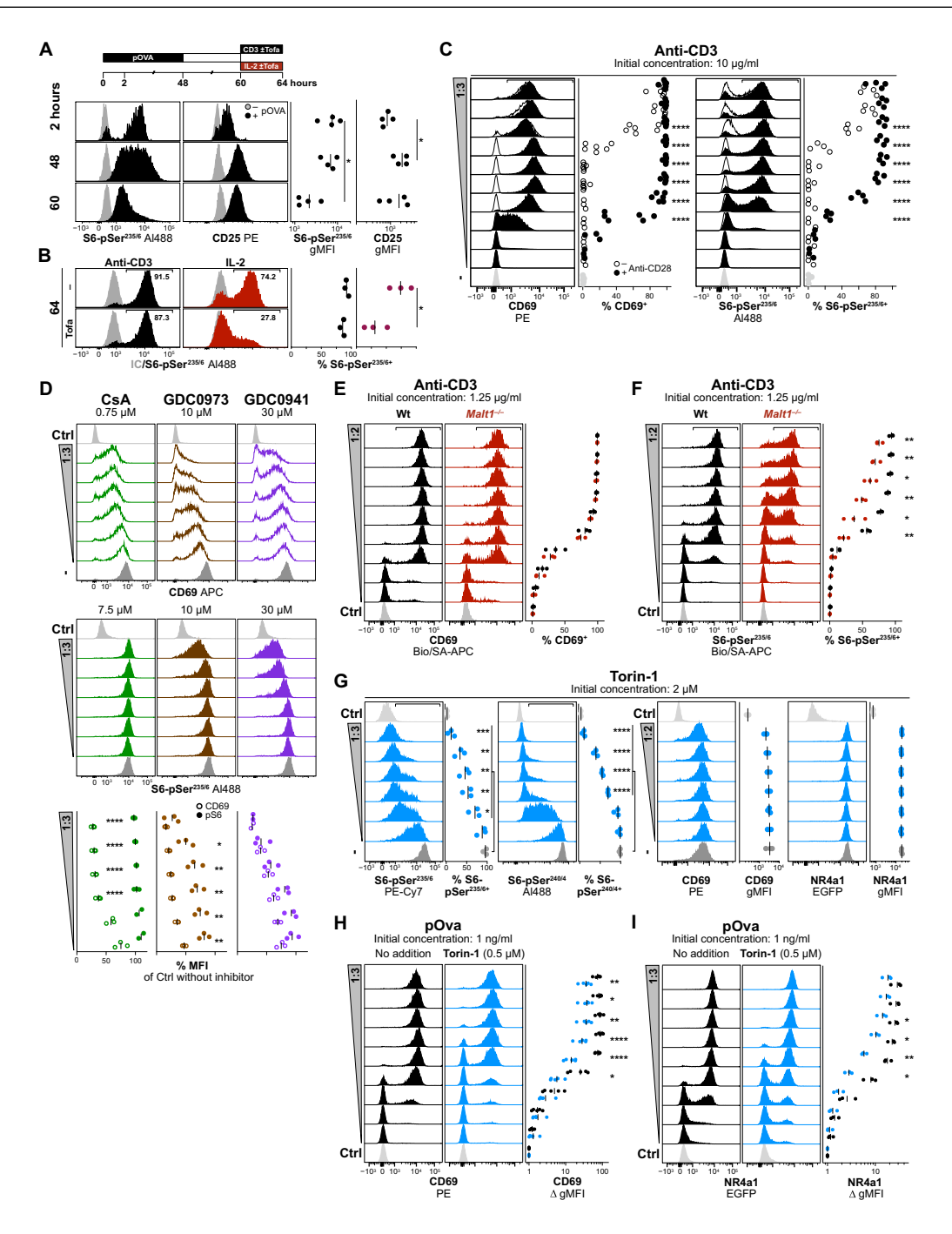


Fig. 2. Cross-talk between conventional and mTORC1 signaling in response to IL-2, CD28, and TCR stimuli. (**A**) Analyses of S6 phosphorylation at Ser^{235/6} and CD25 expression of OT1 T cells stimulated with OVAp (10 ng/ml) for 48 hours and rested overnight. Gray histograms indicate isotype Ctrl (IC) antibodies. CD8⁺T cells from N = 4 animals per group were analyzed. (**B**) The cells in (A) were restimulated with immobilized CD3 (10 μg/ml; left) or IL-2 (10 μg/ml; right) in the presence or absence of 1 μM tofacitinib (Tofa; red). Cells from N = 3 animals per genotype were analyzed. (**C**) B6T cells were stimulated for 16 hours by titrated concentrations of immobilized anti-CD3 antibodies in the absence (open histograms and symbols) or presence (filled) of anti-CD28 (10 μg/ml). CD4⁺T cells from N = 3 to 6 (left) and N = 3 or 4 (right) animals per genotype were analyzed. (**D**) OT1 T cells were stimulated with OVAp (10 ng/ml) for 2 hours in the presence of titrated amounts of cyclosporin A (CsA; left), the MAPK kinase 1 inhibitor GDC0973 (middle), and the Pl3K inhibitor GDC0941 (right). Cells from N = 3 animals per genotype were analyzed for CD69 expression (top) and S6-Ser^{235/6} phosphorylation (bottom). (**E** and **F**) B6 and $Malt1^{-/-}$ T cells were stimulated for 16 hours with graded amounts of immobilized anti-CD3 antibodies and anti-CD28 (5 μg/ml) and analyzed for CD69 expression (E) and S6-Ser^{235/6} phosphorylation (F). CD4⁺ T cells from N = 4 animals per genotype were analyzed. (**G**) Histograms show S6-Ser^{235/6} and S6-Ser^{240/4} phosphorylation (left), CD69 (middle), and NR4a1 reporter expression (right) of OT1 T cells after an overnight OVAp (10 ng/ml) stimulation with titrated Torin-1. CD8⁺ cells from N = 3 animals per genotype were analyzed. (**H** and **I**) CD69 (G) and NR4a1-EGFP (H) expression of OT1 T cells with and without 500 nM Torin-1 after stimulation with titrated OVAp (10 ng/ml) to 0.1 pg/ml). CD8⁺ cells from N = 5 (H) and N = 3 (I) animals per genotype were anal

MAPK pathway has a stronger effect on conventional than on mTORC1dependent signaling, whereas the CBM/NF-κB pathway affects mTORC1 signaling more than conventional TCR signaling. However, mTORC1/2 inhibition with the adenosine 5'-triphosphate-competitive Torin-1 compound, which fully inhibits mTOR activity [(79) and Fig. 2G], did not affect CD69 or NR4a1 abundance, both of which are targets of conventional TCR signaling (4, 6), in response to high levels of OVAp activating the OT1 TCR (Fig. 2G). We thus asked whether mTORC1/2 signaling affected TCR signaling in response to limiting amounts of antigen, a situation more likely to be encountered in responses to pathogens. Torin-1 inhibition lowered the sensitivity of the OT1 TCR three- to ninefold as assessed by CD69 (Fig. 2H) and NR4a1 abundance (Fig. 2I), indicating that mTORC1/2 signaling can affect conventional TCR signaling when antigen quantity is limiting. In summary, these data show that mTORC1/2 activity integrates signals initiated by TCR, IL-2R, and CD28 costimulation and can quantitatively affect conventional TCR signaling. mTORC1/2 thus acts to integrate conventional TCR signals and can also adjust the threshold of T cell activation in case of limiting antigen availability.

mTORC1 regulates RNA synthesis

Initially, lymphocytes were identified as the agents of adaptive immunity in parent-into-F1 graft-versus-host disease experiments by their increasing size, developing prominent nucleoli, and becoming "pyroninophilic" before they begin to divide (80, 81). Because macromolecular biosynthesis is the primary task of rapidly dividing lymphocytes, we asked how deletion of mTORC1 or mTORC2 affected cellular RNA, as assessed by visualizing its proxy double-stranded RNA with the intercalating dye Pyronin in flow cytometry (82-85). After T cell activation, the amount of RNA per cell increased by about ninefold in WT and *Rictor*^{CD4} T cells, whereas the absence of mTORC1 reduced it by about one-half (Fig. 3A). RNA expression differed between the G₀ and G₁ phases of the cell cycle in WT and Rictor^{CD4} T cells. However, Raptor^{CD4} T cells entered the S phase with less RNA per cell without passing through a proper G₁ phase (Fig. 3A). These differences became evident 18 to 48 hours after stimulation (Fig. 3B). When cellular RNA was purified from naive and activated CD4⁺ and CD8⁺ T cells, the amounts of total (Fig. 3C, left) or 28S rRNA (Fig. 3C, right) per cell were increased even more (25- to 47-fold) by activation and again reduced by one-half by Raptor deletion. The difference between the results is likely caused by the use of Pyronin in fixed and permeabilized cells in which doublestranded RNA is unlikely to be entirely accessible to an intercalating dye, thus resulting in underestimation. These data show by different techniques that the amount of RNA per cell is not stable but fluctuates in the process of T cell activation.

TCR-stimulated *Raptor*^{CD4} T cells showed decreased phosphorylation of Thr³⁸⁹ in p70 S6K1 (Fig. 3D), a prominent target of the mTOR kinase in mTORC1 (*51*, *86*). The remaining signal detected in Raptor^{CD4} T cell extracts by the antibody (Fig. 3D, top row) is likely caused by the incomplete CD4-cre-mediated loxP site recombination of both *Raptor*^{fl} alleles in some of the T cells. Such remaining WT signals have been occasionally seen before in proliferation (Fig. 1E) and RNA visualization assays (Fig. 3A). S6K1 and S6K2 phosphorylate S6 at Ser²³⁵, Ser²⁴⁰, Ser²⁴⁴, and Ser²⁴⁷ (*69*, *70*). Two cytometry-compatible antibodies specific for pSer^{235/6} or pSer^{240/4} are commonly used as indirect readouts of mTORC1 activity. We found that these phosphorylation sites were detectable by Western blot analysis of activated T cells from either *Raptor*^{CD4} or *S6K1*/2^{-/-} animals (Fig. 3D), which are viable on a

mixed B6;129 background (87, 88). Analyses by flow cytometry, the dynamic range of which is better suited for the quantification of rare events, indicated that phosphorylation at both pairs of sites is almost entirely attenuated in T cells from $Raptor^{CD4}$ animals but only partially in $S6K1/2^{-/-}$ T cells (Fig. 3, E and F). The remaining activity was most likely mediated by proteins encoded by members of the Rps6ka1 to Rps6ka6 gene family (74, 88) because it was inhibited by BRD7389 (Fig. 3, E and F) (89, 90). However, $S6K1/2^{-/-}$ T cells showed no differences in RNA up-regulation upon TCR stimulation, indicating that rRNA biosynthesis in T cells is not mediated by these kinases (Fig. 3G). We conclude that the TCR-initiated serine phosphorylation of S6 is mediated by mTORC1 and several S6 and RSK family members. S6 phosphorylation itself has no effect on proliferation, as shown for T cells from $S6^{P-/-}$ knock-in mice in which the five S6 Ser residues are replaced with Ala (91).

To identify RNA biotypes that are regulated in an mTORC1-dependent manner, we sequenced precipitable RNA from naive and activated WT and *Raptor*-ablated CD4⁺ and CD8⁺ T cells. The analysis of the RNA biotypes revealed that their relative percentages did not generally differ regarding cell type, genotype, or activation status (Fig. 4A), with three exceptions being mRNA in WT CD8⁺ and rRNA in *Raptor*^{CD4} CD4⁺ and CD8⁺ T cells. In all cell types, ~85% of the RNA matched the 47S pre-rRNA, whereas ~5% was proteincoding mRNA. The next abundant biotype was the small nucleolar RNA, which contributes to the processing of ribosomal RNA and tRNA in the nucleolus. These data indicate a global enhancement of transcription, reminiscent of hypertranscription described not only in cells undergoing developmental transitions such as zygotes, preimplantation epiblasts, and embryonic stem cells but also in adult organ renewal and tumorigenesis (92, 93).

The distribution of the reads over the consensus 45-kb rDNA tandem repeat in the mouse (94) identified the 12.8-kb 47S pre-rRNA, with its regions incorporated into mature ribosomes at higher levels (Fig. 4B). We also found that sequences of the intergenic spacer (IGS) were transcribed, most likely by RNA Pol II, as found previously in tumor cells (95, 96). However, T cell subset, stimulation, and genotype did not affect IGS transcription (Fig. 4C), making a role of such transcripts in T cell activation unlikely. mRNAs of genes contributing to nucleotide and ribosomal biosynthesis and processing were expressed by activated cells in an mTORC1-dependent manner (Fig. 4D).

To assess changes in rRNA processing in T cell activation, we analyzed the reads matching the eight regions of the primary 47S rRNA transcript in more detail. Differences mostly mapped to the external and internal spacers (ETS, ITS-1, and ITS-2) and correlated with activation status rather than genotype (Fig. 4, E and F). This result indicates that the consecutive removal of the 3' ETS, the 5' ETS, and both ITS proceeds independently of mTORC1 (Fig. 4E), which agrees with previous data in tumor cell lines and obtained with chemical mTOR inhibition (97). However, four regions were overrepresented in activated T cells: the 5' ETS-1 stretch 5' of the A' cleavage site [following the nomenclature in (98)], ITS-1, ITS-2, and the 3' ETS (Fig. 4F). The 1.6- to 2.5-fold increases indicate that rRNA processing might be a bottleneck in activated T cells. The only mTORC1-dependent difference that was detectable was a 1.5-fold reduction of 5' ETS-2 reads in stimulated Raptor^{CD4} CD8⁺ T cells (Fig. 4G). Ribosomal biosynthesis is particularly sensitive to imbalances in the abundance of its components as indicated by ribosomopathies caused by haploinsufficient ribosomal or ribosomal biogenesis proteins (99, 100). The identity

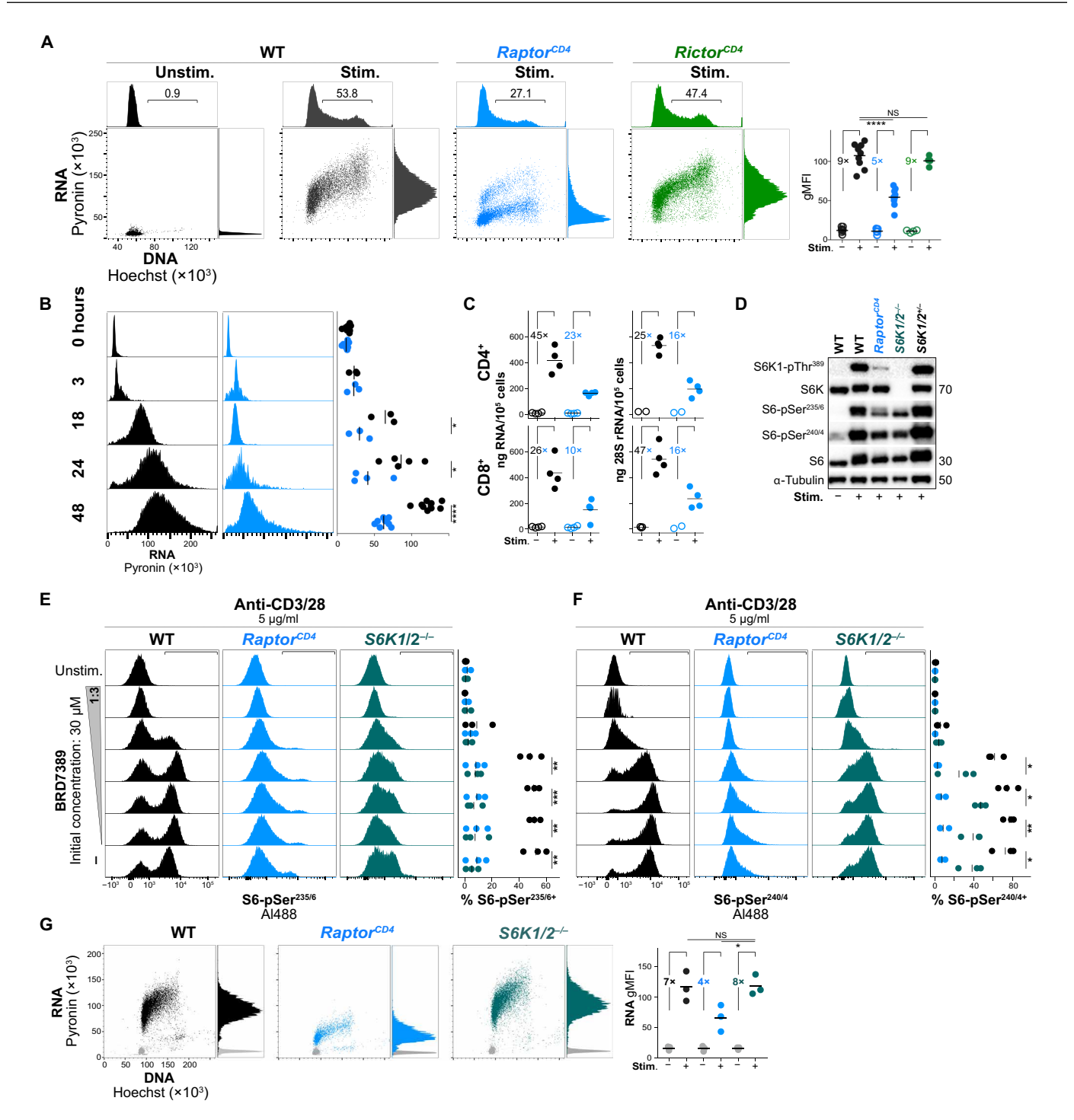


Fig. 3. mTORC1 restricts the expression of cellular RNA, but mTORC2 and S6K1/2 do not. (**A**) DNA and RNA amounts of OT1 T cells of the indicated genotypes were determined after 2 days in culture without (unstim.) or with OVAp (10 ng/ml) (stim.). Percentages in DNA plot indicate the cells in S, G_2 , and M phases of the cell cycle. RNA gMFI is shown on the right. CD8⁺ cells from N = 9 (WT and $Raptor^{CD4}$) and N = 4 ($Rictor^{CD4}$) animals were analyzed. (**B**) RNA content of WT and $Raptor^{CD4}$ OT1 T cells after OVAp stimulation over time. CD8⁺ cells from N = 3 to 9 animals per genotype were analyzed. (**C**) Measurements of RNA amounts in CD4⁺ and CD8⁺ WT and $Raptor^{CD4}$ T cells after 2 days in culture without or with stimulation by immobilized CD3/CD28 antibodies (left) and 28S rRNA measurements by electrophoretic chromatography (right). RNA samples of cells from N = 4 (left) and N = 2 to 4 (right) animals per genotype were analyzed. (**D**) Sorted T cells were stimulated with anti-CD3 and anti-CD28 antibodies for 16 hours and their proteins probed for phosphorylation at the three sites: S6K1-Thr³⁸⁹, S6-Ser^{235/6}, and S6-Ser^{240/4}. The experiment was repeated twice with similar results, using cells from different animals each time. (**E** and **F**) Sorted T cells were stimulated for 2.5 hours as in (D) in the presence of 0.3 to 30 μM BRD7389 and analyzed for S6-Ser^{235/6} (E) and S6-Ser^{240/4} (F) phosphorylation. CD8⁺ cells from N = 3 animals per genotype were analyzed. (**G**) DNA and RNA amounts of sorted T cells of the indicated genotypes were stimulated and analyzed for DNA and RNA as in (A). Unstimulated cells are depicted in gray. CD8⁺ cells from N = 3 animals per genotype were analyzed. *P < 0.05, **P < 0.01, ***P < 0.001, and ****P < 0.0001 by unpaired two-tailed Student's t test. NS, not significant.

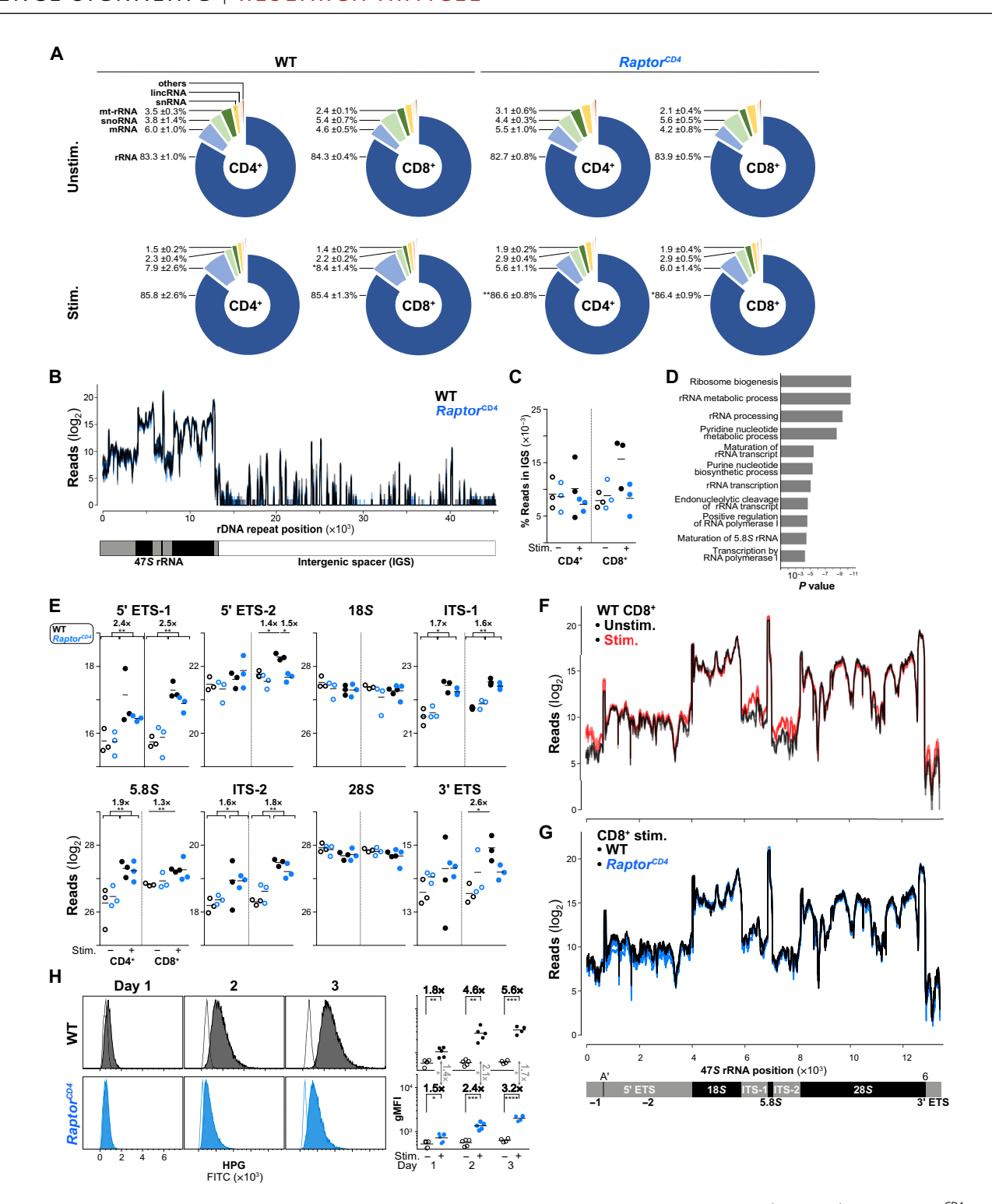


Fig. 4. RNA biotypes and rRNA transcription and processing in T cells. (A) RNA biotypes identified by sequencing in CD4⁺ and CD8⁺ WT and $Raptor^{CD4}$ T cells after 2 days in culture without or with stimulation by immobilized CD3/CD28 antibodies. Means \pm SD are shown. snoRNA, small nucleolar RNA; lincRNA, long intergenic noncoding RNA; snRNA, small nuclear RNA. (**B**) Reads across the consensus rDNA repeat in activated CD8⁺T cells of the indicated genotypes. (**C**) Comparisons of reads in the IGS across all samples. (**D**) mTORC1-dependent GO pathways enriched in activated CD8⁺T cells. (**E**) Numbers of reads over eight regions of the 47S pre-rRNA. Indicated are fold changes. (**F**) Comparison of 47S rRNA tracks of WT CD8⁺ unstim. (black) compared with stim. (red) T cells. (**G**) Comparison of 47S rRNA tracks of CD8⁺ stim. WT (black) compared with $Raptor^{CD4}$ (blue) T cells. In (A) to (G), sorted cells from N = 3 animals per genotype and condition were analyzed. (**H**) Translational activity of AND CD4⁺T cells of the indicated genotypes stimulated by anti-CD3/CD28 antibodies, washed, and cultured in methionine-free HPG-containing medium at the indicated time points. HPG incorporation was quantified 1 hour later. Open histograms and symbols indicate unstimulated cells. CD4⁺T cells from N = 5 or 6 animals per genotype were analyzed. *P < 0.00, *P < 0.0

of the nucleases removing the ETS and ITS sequences remains unknown (54, 98), but the 5' ETS-A region is bound by fibrillarin for subnucleolar sorting, and the 3' ETS is removed with the help of the unhealthy ribosome biogenesis 1 (URB1) protein and the U8 small nucleolar RNA (101, 102). In summary, these results suggest that the amount of rRNA per T cell is controlled by Pol I-dependent pre-rRNA transcription rather than by 47S rRNA processing. However, the relative increase in processing intermediates indicates an upper limit on ribosomal biosynthesis and perhaps the rate of T cell clonal expansion.

Ribosomal activity was assessed by incorporation of the cell-permeable and clickable methionine analog homopropargylglycine (HPG) into nascent protein chains. Translational activity increased over time but was reduced to ~50% in Raptor-deleted T cells (Fig. 4H). Thus, in T cell activation, the reduced amount of RNA per cell in the absence of mTORC1 (Fig. 3, A to C and G) is coupled with diminished translation.

mTORC1 controls nucleolar activity and structure and cell volume

To visualize rRNA biosynthesis, we designed 48 oligonucleotide fluorescence in situ hybridization (FISH) probes that bind to the 5' ETS (table S1), which, in tumor cells such as HeLa cells, is cleaved and destroyed within minutes after rRNA synthesis (103). The ~200 47S pre-rRNA genes in mice are distributed in large tandem arrays on chromosomes 12, 15, 16, 18, and 19, and the probes were built using a consensus sequence of these genes (94). The probes thus visualize the nascent 47S pre-rRNA transcript and its first intermediate missing the 3' ETS (104, 105). Activation by antigen led to a ~10-fold induction of 5' ETS rRNA in WT and Rictor CD4 OT1 T cells but only an ~5-fold induction in *Raptor*^{CD4} cells. Overall, polyadenylated mRNA expression was affected to a lesser extent by the absence of mTORC1 than rRNA transcripton was (Fig. 5A). These data correlate Pol I-dependent rRNA gene transcription visualized by 5' ETS FISH and RNA quantification with Pyronin in activated T cells.

rRNAs are synthesized, processed, and assembled with 79 ribosomal proteins to the large 60S and small 40S ribosomal subunits. The process is assisted by ~300 proteins in the largest nuclear substructure, the nucleolus, whose multiple functions are accompanied by multiphase condensates and liquid-liquid phase separation (58, 106-108). We thus explored how the activity of Pol I, found in the fibrillar center of the nucleolus (107, 109), is affected by mTORC deficiencies using ImageStream cytometry. Figure S3 shows how T cells were pregated on the basis of imaging parameters. In ImageStream cytometry using 5' ETS-specific FISH probes, the number and size of the fibrillar centers peaked on day 1 and decreased over the next 2 days in both WT and Rictor^{CD4} T cells. In contrast, the increase in both parameters in Raptor^{CD4} T cells was delayed over this period so that on day 3, the fibrillar centers were more numerous and covered a larger area than in control cells that had already reduced fibrillar centers to the starting number (Fig. 5B). Thus, mTORC1 deficiency, but not mTORC2 deficiency,

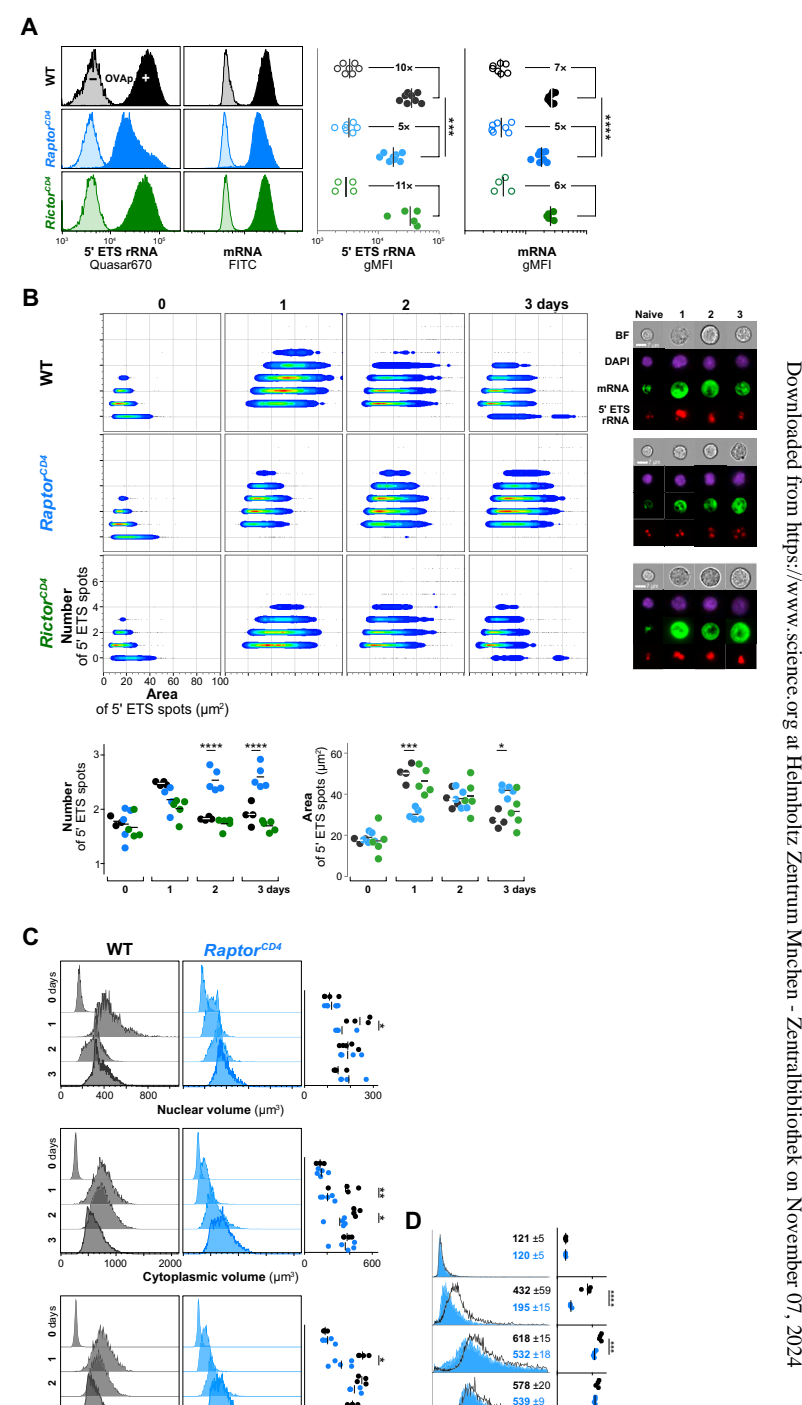


Fig. 5. mTORC1 controls nucleolus numbers and structure. (A) 5' ETS RNA FISH probe (left) and oligo(dT) (right) staining of unstimulated (shaded) and stimulated (solid) OT1 cells of the indicated genotypes. $CD8^+T$ cells from N=4 to 7 animals per genotype were analyzed. (B) Visualization of 5' ETS rRNA in stimulated OT1 cells over time by imaging flow cytometry. CD8+T cells from N = 4 or 5 animals per genotype were analyzed. Scale bars, 7 μ m. (C) Nuclear, cytoplasmic, and cellular volumes determined by imaging cytometry over time in WT and Raptor CD4 OT1 T cells. $CD8^+T$ cells from N = 4 to 6 animals per genotype were analyzed. BF, bright-field. (D) Volumes of unfixed cells determined by electronic impedance. Numbers indicate the average cell size \pm SD. Sorted CD8⁺ T cells from N = 3 animals per genotype were analyzed. *P < 0.05, **P < 0.01, ***P < 0.001, and ****P < 0.0001 by unpaired two-tailed Student's t test.

Cellular volume (um3)

1000 1500

causes a delay in Pol I activity and parameters of nucleolar structure over the first days of T cell activation.

The increase in cellular volume, which is a combination of nuclear and cytoplasmic volumes, was delayed in a similar manner in *Raptor*-deleted T cells (Fig. 5C, left). Volumetric Coulter impedance measurements of unfixed live cells to measure cell size (*110*) showed the fivefold increase in WT cells of ~120 to ~620 fl, which was delayed by the absence of mTORC1 (Fig. 5D). These changes are consistent with electron microscopic measurements (*111*). Thus, T cells lacking mTORC1 cannot adjust rRNA synthesis and consequently cannot calibrate nucleolar and cellular structures sufficiently to the demands posed by rapid cell division.

mTORC1 accelerates each division of the expansion phase by promoting rRNA transcription and cell cycle checkpoint transitions

Having seen the effects of mTORC1 but not mTORC2 ablation on nucleolar structure and function, we asked how chemical mTOR inhibition would affect RNA synthesis and proliferation at different time points of clonal expansion. rRNA transcription was entirely blockable when Torin-1 was added from the beginning of T cell activation and less so at later time points (Fig. 6A). Cell division was hampered by late Torin-1 addition as well, suggesting an important role for mTORC in T cell expansion beyond the exit of quiescence (Fig. 6, B and C), with the amount of RNA per cell reduced accordingly (Fig. 6D). These data show that mTORC activity affects each consecutive cell division and are consistent with the reduced division rates of later divisions of Raptor-deleted T cells in vivo (Fig. 1, A to D). Thus, the Torin-1 effects are most likely caused by the inhibition of mTORC1 and not of mTORC2. The Torin-1-mediated delay in T cell division was reversible such that both proliferation and RNA amounts per cell reached levels similar to those in uninhibited cells upon Torin-1 removal (Fig. 6, E and F). Cell cycle analyses indicated that late mTORC1 inhibition hampered primarily the G₁-S transition, leading to more Raptor-deleted T cells in the G₁ phase and fewer cells in the S, G2, and M phases (Fig. 6G). However, among the cells in G₂ and M phases, fewer were the M phase, indicating a second mTORC-dependent restriction point at the G2-M transition (Fig. 6H), just as we had seen with Raptor-depleted T cells (Fig. 1F). Together, these data show that in proliferating T cells, mTORC1 promotes each consecutive cell division by facilitating both rRNA transcription and passage through the G₁-S and G₂-M transition points.

RNA Pol I activity controls both cell cycle and mTORC1 activity

To further understand the causal relationships among cell cycle progression, mTORC1 activity, and Pol I-dependent transcription, we inhibited Pol I transcription with quarfloxin (also known as CX-3543), which interferes with the binding of the transcription factor SL1 to the 47S rDNA promoter (112). 5' ETS rRNA expression was entirely blocked when quarfloxin was present in the first 24 hours of T cell stimulation but not when added 48 hours later (Fig. 7A). This result indicates storage of presynthesized 47S rRNA in an unprocessed form once rRNA transcription is blocked, which has been described in yeast and tumor cells (54, 113). Quarfloxin also inhibited T cell proliferation when added later, indicating the ongoing dependence of T cell division on Pol I-dependent transcription (Fig. 7B). The cells were arrested in the G₁ and G₂-M phases, leading to depletion of cells in S phase

(Fig. 7C). These data are reminiscent of not only the partial cell cycle inhibition at the G_1 -S transition point but also that at the G_2 -M transition point caused by the absence or inhibition of mTORC1 (Figs. 1F and 6, G and H). Blocking Pol I in a distinct manner with BMH-21, which causes proteasome-dependent degradation of Pol I component RPA194 (*114*), arrested the proliferating T cells in G_1 and G_2 -M as well (Fig. 7D, top), corroborating the previous conclusion. The percentage of cells in M phase, as indicated by Ser²⁸ phosphorylation of histone H3, was reduced sixfold, indicating the necessity of rRNA transcription for the initiation of T cell mitosis (Fig. 6H). These data show that T cell proliferation requires Pol I activity at the G_1 -S and G_2 -M transition points of the cell cycle.

We noticed that quarfloxin inhibited forward scatter, suggesting feedback to mTORC1 (Fig. 7E, left). We found that quarfloxin inhibited mTORC1 activity, as indicated by the decrease in the phosphorylation of Ser^{235/6} and Ser^{240/4} in S6, with a half-maximal inhibition at ~125 nM for pSer^{235/6} and at a slightly higher concentration for pSer^{240/4} (Fig. 7E, middle and right). We also confirmed the inhibition of mTORC1 activity by Western blotting for the phosphorylation of the direct target Thr³⁸⁹ in S6K1. mTOR, Raptor, and Rictor proteins themselves remained unchanged by the addition of quarfloxin (Fig. 7F). These data indicate an enhancement of mTORC1 activity by Pol I–dependent transcription. The tight coregulation of rRNA transcription and mTORC1 activity was corroborated by the parallel decrease in 5′ ETS rRNA and S6 phosphorylation within hours of application of quarfloxin (Fig. 7G) and BMH-21 (Fig. 7H). Thus, the cell cycle, mTORC1 activity, and rRNA transcription are interlinked and mutually dependent.

DISCUSSION

Our data let us make five points. First, there was mutual regulation between conventional TCR-dependent and mTORC1-dependent signaling, which has been appreciated only occasionally (75). Besides the classical mTORC1 targets 4E-BP1/2 and S6K1/2, at least 326 proteins are phosphorylated in an mTORC1-dependent manner in T cells, including MAPK, NF-κB, and NFAT components (51). Reciprocally, we learned that Malt1^{-/-} T cells, which lack the CBM/NF-κB pathway, showed reduced mTORC1 activity, especially in response to limiting TCR stimulation (Fig. 2, E and F). Because mTORC1/2 affects TCR sensitivity (Fig. 2, H and I), it is likely a hub that integrates antigen recognition, cytokine signals, and nutrient availability to adjust the degree of clonal expansion. It remains unclear how mTORC1 regulates Pol I activity and ribosomal biosynthesis in lymphocytes. In other contexts, they are not necessarily linked: In Drosophila germline stem cells, Tor activation and ribosomal biosynthesis can be uncoupled, which promotes terminal differentiation (115). Because S6K1 and S6K2 regulate ribosomal protein synthesis in hepatocytes in response to food intake (87), it can be concluded that the role of S6K1/2 in transmitting mTORC1-derived signals differs between tissues of mice. Our exclusion for a role for S6K1 and S6K2 agrees with earlier findings of normal cell growth and proliferation of lymphocytes from S6K hypomorphs (63). Although the mTORC1-dependent phosphorylation of the Pol I-specific transcription factors Rrn3 (RNA polymerase I transcription factor homolog 3, also known as TIF-1A) and Ubtf (upstream binding transcription factor, also known as UBF) has been detected in activated T cells (51), it is expected that additional factors are involved (104).

Second, mTORC1 functionality is effective beyond the initial division after the exit from quiescence in vivo. Deficiency of mTORC1

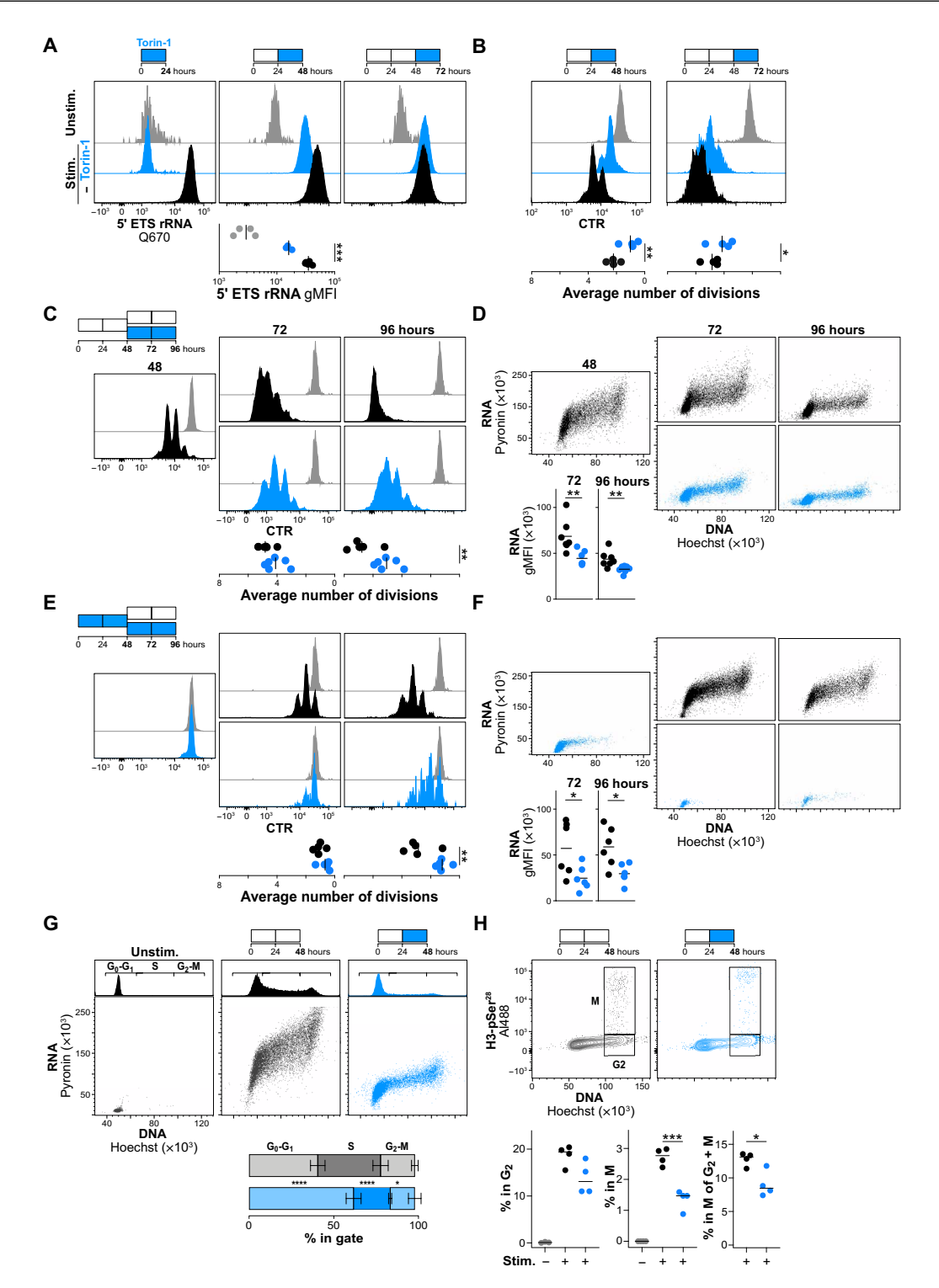


Fig. 6. The role of mTORC1 in RNA expression and subsequent cell divisions. (**A**) 5' ETS RNA expression in OVAp-stimulated OT1 cells before and after the addition of 1 μ M Torin-1 (blue). Time points in bold indicate time of analysis. Cells from N=3 to 5 animals were analyzed. (**B**) Effect of Torin-1 on proliferation of OT1 cells when added after the initiation of proliferation. Cells from N=4 animals were analyzed. (**C** and **D**) Effect of late mTORC1 inhibition on proliferation (C) and RNA biosynthesis (D). The addition of Torin-1 is indicated in blue. Cells from N=6 (C) or N=7 (D) animals were analyzed. (**E** and **F**) Effect of Torin-1 withdrawal after 48 hours of stimulation on proliferation (E) and RNA expression (F). Cells from N=5 (E) or N=6 (F) animals were analyzed. (**G**) Effect of mTORC1 inhibition on the numbers of cells in G_0 - G_1 , G_1 , G_2 - G_2 0 phases. Cells from G_2 1 and G_3 2 phases. Cells from G_3 3 and G_3 4 phases. Cells from G_3 4 animals were analyzed. (**B**) Effect of G_3 5 and G_3 6 phases. Cells from G_3 6 phases. Cells from G_3 7 and G_3 8 phases. Cells from G_3 8 phases.

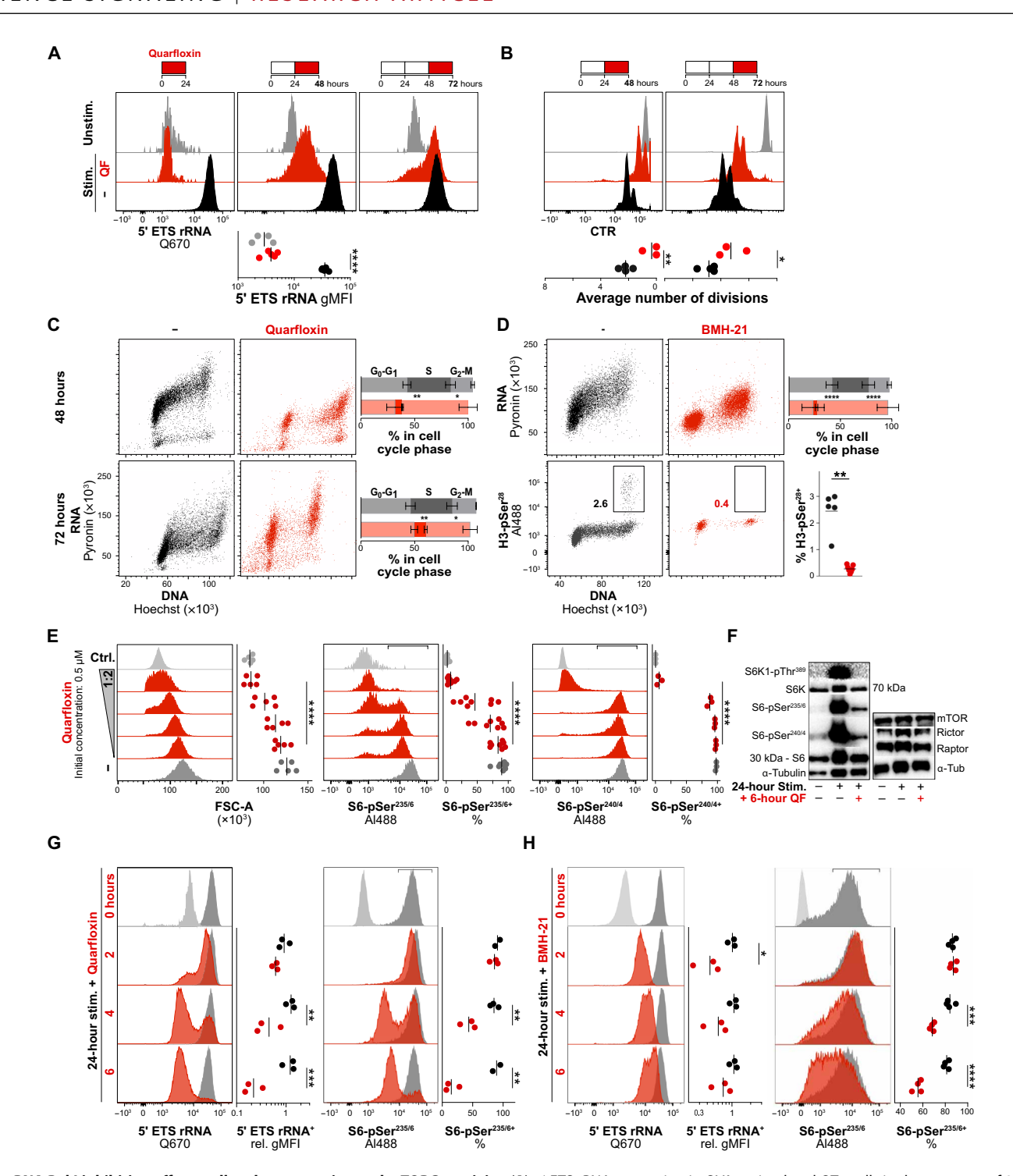


Fig. 7. RNA Pol I inhibition affects cell cycle progression and mTORC1 activity. (A) 5' ETS rRNA expression in OVAp-stimulated OT1 cells in the presence of 200 nM quarfloxin (QF; red). Cells from N = 4 animals were analyzed. **(B)** Proliferation of OT1 cells with quarfloxin added at indicated time points. Cells from N = 3 or 4 animals were analyzed. **(C)** Cell cycle analysis of OT1 cells treated as in (A) at 48 hours (top) and 72 hours (bottom). Cells from N = 3 animals were analyzed. **(D)** Cell cycle analysis of OT1 cells treated 24 hours with 750 nM BMH-21. Bottom panels show H3-pSer²⁸ staining of cells treated with 750 nM BMH-21 on day 3 to measure the percentage of cells in mitosis. (C) and (D) show 2-day (top) and 3-day (bottom) cultures. Cells from N = 7 (top) and N = 5 (bottom) animals were analyzed. **(E)** Effect of quarfloxin after 16 hours of stimulation on cell growth and S6-Ser^{240/4} phosphorylation. Cells from N = 5 (left and middle) and N = 3 (right) animals were analyzed. FSC-A, forward scatter area. **(F)** Purified OT1 cells were stimulated for 30 hours with anti-CD3/CD28, and dimethyl sulfoxide (–) or 2 μ M quarfloxin was added for the last 6 hours before cells were subjected to Western blot analysis for phosphorylation of S6K1-Thr³⁸⁹, S6-Ser^{225/6}, and S6-Ser^{240/4}. The results are representative of three independent experiments. **(G** and **H)** Analysis of 5' ETS rRNA transcription and S6-Ser^{235/6} phosphorylation of OT1 cells stimulated for 24 hours before being treated with 2 μ M quarfloxin (G) or 750 nM BMH-21 (H) as indicated. Cells from N = 3 animals were analyzed. *P < 0.05, **P < 0.01, **P < 0.001, and ****P < 0.0001 by unpaired two-tailed Student's t test.

slowed down the cell cycle of each consecutive division of both CD4⁺ and CD8⁺ T cells in their expansion phases. This was confirmed with *Raptor*-deleted T cells in vitro and by the late addition of Torin-1 after the initial one or two divisions were completed. Torin-1 slowed the following divisions and reduced the rRNA expression. Although these results agree with a report on delayed proliferation of mTOR-deleted T cells in a high-dose vaccinia infection (*61*), they contrast with some of the data supporting the view that mTORC1 matters exclusively for the first division (*32*, *116*) and make therapeutic mTORC1 inhibition to treat autoimmune and inflammatory diseases after manifestation more plausible (*38*, *117*).

Third, the macromolecular density in the cytosol changes over the course of T cell activation mostly because of massive ribosomal biogenesis. Although the electronic cell volume of WTT cells increased approximately fivefold from 120 to 620 fl, the amount of RNA per cell, 85% of which is rRNA, increased at least ninefold. This agrees with earlier assessments of dry biomass production from 30 to 400 pg by phytohemagglutinin-stimulated lymphocytes (118). This mTORC1dependent approximately twofold increase in cytoplasmic concentration of ribosomes is likely to change the biophysical properties of the cytoplasm. The use of nanoparticles of ribosomal size in tumor cells has revealed that mTORC1 inhibition reduces ribosomal abundance and consequently the effective diffusion coefficient and phase separation properties of the cytoplasm (119). Our data suggest that ribosomal abundance is not a fixed but rather a pliable parameter in the process of T cell activation. Amino acid starvation or rapamycinmediated mTORC1 inhibition affects rRNA transcription in yeast and cancer cells (120-123), and proteomic studies have shown that ribosomal proteins are synthesized in an mTORC1-dependent manner in activated T cells (28, 30).

Fourth, our data showed that it was not the end product but the process of ribosomal biosynthesis itself that affected T cell proliferation. A late 24-hour inhibition of ribosomal biosynthesis by Torin-1 or quarfloxin did not reduce the amount of 47S pre-rRNA as would be expected for a precursor being turned over within minutes to hours in tumor cells (54). Rather, 5' ETS remained detectable even 24 hours after inhibition (Figs. 6A and 7A), suggesting storage of pre-rRNA as has been seen in tumor cells (54). Our data with Pol I inhibition (Fig. 7B) suggested that it was the stalled Pol I activity that delayed the cell cycle in T cells in an mTORC1-dependent manner. In tumor cells, nascent 5' ETS-1 is bound to fibrillarin and sorted through its glycine- and arginine-rich domain, an intrinsically disordered region, into the dense fibrillar component, the nucleolar compartment where rRNA processing occurs (102, 106, 124). The mTORC1-dependent increase in rRNA expression in activated T cells was reflected by nucleolar number and size (Fig. 5B) and likely also affected nucleolar substructures that may serve as immunological biomarkers. The nucleolus is a multifunctional and multiphase condensate that recruits proteins during the cell cycle, rRNA processing, protein folding, and human disease (101, 106, 109, 125–127), and rRNA transcription is also an important feature of memory T cells (105).

Fifth, our data suggest feedback from nucleolar Pol I activity to mTORC1 activity. Because nucleotide availability restricts Pol I activity, it is to be expected that blocking it would reciprocally lead to increased nucleotide triphosphate levels and improved signaling. A similar mechanism has been shown for glycolytic nucleotide triphosphates affecting PI3K signaling activity (128). However,

the opposite was the case here: Blocking Pol I decreased mTORC1 activity (Fig. 7, G and H). This finding indicates that the nucleolus is more than a passive receiver of TCR initiated signaling but actively participates in it. Although the nature of this signal is unknown, it might be a powerful target for manipulating adaptive immune responses.

The ≥9-fold increase in all RNA biotypes in T cell activation harks back to the concept of hypertranscription observed decades ago in transitional processes as diverse as zygotic cell division, hematopoietic stem and progenitor cell expansion, regeneration, and cancer (92, 93). Here, we suggest it as a mechanism that might offer insights into the rapid biomass production required for T cell clonal expansion.

MATERIALS AND METHODS

Mice

B6.C-H2-K^{bm1}/ByJ (stock number 001060) and B6.C-H2-Ab1^{bm12}/ KhEgJ (stock number 001162) mice were obtained from Jackson Laboratories. B10.BR mice were purchased from Jackson Laboratories (B10.BR-*H2*^{k2} *H2-T18*^a/SgSnJJrep, 004804) or Envigo (B10. BR-H-2^{k2}/OlaHsd). iMCC animals carry the transgenes Ii-rTA [Tg (Cd74-rtTA)#Doi] and TIM [Tg (tetO-Cd74/MCC)#Doi] (129), and iOVA animals carry the Ii-rTA and TSO [Tg (TetO-OVA)7Obst] transgenes (66). AND [Tg (TcrAND)53Hed] and OT1 [Tg (Tcra Tcrb)1100Mjb] TCR transgenic mice carry the CD45.1 encoding allogenic marker *Ptprc^a* originally derived from B6.SJL-*Ptprc^aPepd^o/* BoyJ animals (66). NR4a1-enhanced green fluorescent protein (EGFP) transgenics [Tg (Nr4a1-EGFP/cre)820Khog, 016617] were purchased from Jackson Laboratories and backcrossed to OT1⁺ and Ptprc^a mice. Animals carrying the CD4-cre transgene [Tg (Cd4-cre)1Cwi, 017336], loxP-flanked Raptor (B6-Rptor tm1. IDmsa, 013188), and Rictor (B6.Rictor^{tm1.1Klg}, 020649) loci were obtained from Jackson Laboratories and are named $Raptor^{CD4}$ and $Rictor^{CD4}$, respectively. $S6K1/2^{-/-}$ ($Rps6kb1^{tm1Gtho}$; $Rps6kb2^{tm1Gtho}$) animals were obtained from M. Pende (Institut Necker Enfants Malades, Université de Paris, France) and are kept on a mixed C57BL/6 J;129P2/OlaHsd background (87, 88). $Malt1^{-/-}$ [Malt1^{tm1d(EUCOMM)Hmgu}] mice lack exon 3, resulting in a downstream frameshift (77). Mice of both sexes were used at 6 to 18 weeks of age. All mice were genotyped by polymerase chain reaction or by cytometry and housed in groups of two to five animals per cage in specific pathogen-free facilities at the Institute for Immunology or at the specific and opportunistic pathogen-free facilities of the Core Facility Animal Models at the Biomedical Center of LMU Munich. Animal care was in accordance with institutional guidelines, and experimental procedures were approved by the Government of Upper Bavaria, Germany, protocols 55.2-1-54-2532-84-2015 and 55.2-2532.Vet_02-21-4.

Animal treatments and adoptive transfers

Recipients of adoptively transferred T cells (Fig. 1, A to D) were treated intraperitoneally with 20 or 40 µg of anti-CD40 [clone FGK45.5, catalog number: BE0016-2, Research Resource Identifier (RRID): AB_1107647, Bio X Cell] in 100 µl of phosphate-buffered saline (PBS) to optimize antigen presentation by immunogenic dendritic cells and macrophages to T cells (45, 130). As responder cells, subcutaneous lymph nodes were harvested and labeled with Cell-Tracker dyes, and 1×10^6 to 2×10^6 cells were injected intravenously in 100 µl of Dulbecco's modified Eagle's medium (DMEM).

Cell isolation and culture

Lymphocyte single-cell suspensions from the spleen and lymph nodes were purified by Percoll (Pan Biotech) centrifugation at 1500 rpm for 10 min with reduced brake. A total of 2×10^5 OT1 lymphocytes cells per well were cultured in round-bottom 96-well plates (Sarstedt, suspension type) in RPMI 1640 medium containing GlutaMAX (Thermo Fisher Scientific), 10% fetal bovine serum (Pan Biotech or Anprotech), 5 ml of antibiotic/antimycotic (PAA), and 55 μM (2 μl/ 500 ml) β-mercaptoethanol (Roth) and stimulated with OVAp (10 ng/ ml; SIINFEKL, Peptides & Elephants) for the indicated time points. For stimulations with antibodies, lymphocyte suspensions were depleted by magnetic cell sorting through depletion by an incubation with biotinylated antibodies (CD11b, CD11c, TER119, CD45R, CD19, Ly6G/C, CD49b and, if required, CD4 or CD8) for 15 min on ice. After two washing steps, the cells were incubated with anti-biotin-coated magnetic beads (Miltenyi) for 10 min. The suspensions were washed and then sorted into positive and negative fractions using LS columns or an autoMACS (Miltenyi) device. A total of 10⁵ T cells were cultured in round-bottom plates (Sarstedt, suspension type) that were coated with anti-CD3 (clone 145-2C11, catalog no. BE0001-1, RRID: AB_1107634, Bio X Cell; 2 or 10 µg/ml or titrated amounts) and anti-CD28 (37.51, catalog no. BE0015-1, RRID: AB_1107624, Bio X Cell; 10 μg/ml) antibodies for 90 min at 37°C. Where indicated, cells were treated with BMH-21 (catalog no. S7718, Selleckchem), cyclosporin A (AG-CN2-0079-M100, AdipoGen), GDC0941 (G124082, LKT Labs), GDC0973 (G124084.5, LKT Labs), quarfloxin (HY-14776, MedChemExpress), tofactinib (CP-690550, Selleckchem), or Torin-1 (S2827, Selleckchem).

Dye labeling

To visualize cell proliferation, naïve T cells/lymphocytes were labeled with CTV (C34557), CellTracker Deep Red (CTR; C34565), or carboxyfluorescein diacetate succinimidyl ester (CFSE; catalog no. V12883, all Thermo Fisher Scientific). Cells were resuspended in prewarmed PBS/0.5% bovine serum albumin (BSA) at 2×10^7 cells/ ml, and 1 μ l of dye was added while vortexing. Cells were incubated for 10 min in a water bath at 37°C, centrifuged through a fetal bovine serum cushion, and washed twice with fluorescence-activated cell sorting (FACS) buffer (DMEM without phenol red and 0.5% BSA). For in vivo transfers, 1×10^6 to 2×10^6 cells were injected intravenously in 100 μ l of DMEM. The number of divisions was calculated as $N=\log_2(g\mathrm{MFI}_{\mathrm{ctrl}}$ / $g\mathrm{MFI}_{\mathrm{sample}}$), where $g\mathrm{MFI}_{\mathrm{ctrl}}$ and $g\mathrm{MFI}_{\mathrm{sample}}$ are the geometric mean fluorescence intensity of control and sample, respectively.

Flow cytometry

Lymphocytes were harvested from cell culture at different time points, washed, and aliquoted into round-bottom 96-well plates (Diagonal) for staining. Lymphocytes from in vivo experiments were isolated from the spleen and lymph nodes at the indicated time points and aliquoted as well into 96-well plates. The cells were spun, blocked with anti-CD16 (clone 2.4G2, catalog no. BE0008, RRID: AB_1107603) from Bio X Cell, and resuspended in 50 µl of FACS buffer containing antibody mixtures. 4',6-Diamidino-2-phenylindole (DAPI) (Invitrogen) or fixable viability dye eFluor780 (eBioscience) was used to exclude dead cells. The cells were recorded on Canto II or LSRFortessa (BD Biosciences) cytometers. Antibodies CD4–allophycocyanin (APC) (catalog no. 116014, RRID: AB_2563025), CD4-APCCy7 (100414, AB_312699), CD4-biotin (100508, AB_312711), CD4-PECy7 (100422,

AB_312707), CD4-PerCP (100538, AB_893325), CD4-PerCPCy5.5 (100434, AB_893324), CD4-Al488 (100529, AB_389303), CD8-Al647 (100724, AB_389326), CD8-biotin (100704, AB_312743), CD8fluorescein isothiocyanate (FITC) (100705, AB_312744), CD8phycoerythrin (PE) (100707, AB_312746), CD8-PerCP (100732, AB_893423), CD11b-biotin (101204, AB_312787), CD11c-biotin (117304, AB_313773), CD25-PE (101904, AB_312847), CD44-PECy7 (103030, AB_830787), CD45R (103204, AB_312989), CD45.1-Al647 (110720, AB_492864), CD45.1-APC (110714, AB_313503), CD45.1-PECy7 (110730, AB_1134168), CD49b-biotin (108904, AB_ 313411), CD62L-PE (104408, AB_313095), CD69-PE (104508, AB_ 313111), CD90.1-Al647 (202507, AB_492885), H3-pSer²⁸-Al488 (641003, AB_1279417), Ly6G/Ly6C-biotin (108404, AB_313369), TCR-Vα2-Al488 (127820, AB 2687230), and Ter119-biotin (116204, AB_313705) were from BioLegend; TCR-Vβ3-FITC (553208, AB_ 394708) was from BD Biosciences; and S6-pSer^{235/6}-Al488 (clone 2F9, 4854, AB_390782), S6-pSer^{235/6}-PECy7 (D57.2.2E, 4854, AB_ 390782), S6-pSer^{240/4} (D68F8, 5018, AB_10695861), and rabbit isotype Ctrl-Al488 (2975, AB_10699151) were from Cell Signaling Technology. For sorting live cells depleted of necrotic and apoptotic cells, in house-produced recombinant MFG-E8-EGFP, which binds to phosphatidylserine (131), was coupled to magnetic tosylactivated beads (M-450 Dynabeads, Thermo Fisher Scientific) according to the manufacturer's instructions. To remove dead cells, MFG-E8-EGFPcoupled beads were incubated with cell suspensions and placed on a magnet, and unbound nonmagnetic live cells were further processed. Flow cytometry data were analyzed with FlowJo v. 10, and the statistics panel was prepared with GraphPad Prism v. 7 or 10. Because all analyses were considered exploratory, no adjustment for multiple testing was performed. Electronic cell volumes were determined with a CASY Counter (Omni Life Science), exported from its CASYworX software v. 1.26, and visualized in Prism.

DNA and RNA staining

A total of 1×10^6 T cells were stained for surface markers and fixed in 4% paraformaldehyde. The cells were then permeabilized with Perm Buffer III (catalog no. 558050, BD Biosciences), washed twice, resuspended in 100 µl of Hoechst 33342 (10 µg/ml; H3570, Thermo Fisher Scientific) in PBS, and incubated for 10 min at room temperature in the dark. Then, 100 µl of pyronin Y (P9172-1G, Merck) solution (5 µg/ml in PBS, freshly prepared from a stock of 1 mg/ml) was added, and the cells were incubated for 10 min. Cells were centrifuged and resuspended in FACS buffer and immediately measured on an LSRFortessa cytometer. Care was taken to stain all samples at 10^6 cells/ml to minimize MFI variability. Voltage (305 nm) was adjusted to a standard MFI of 50,000 for the N=2 peaks before acquisition if required.

5' ETS rRNA FISH staining

A total of 1×10^6 to 3×10^6 cells were stained for cell surface markers, fixed with 4% paraformal dehyde, and permeabilized in Perm Buffer III (BD Biosciences). Cells were washed once in Wash Buffer A (WA1-60, Stellaris), followed by overnight incubation in 100 µl of hybridization buffer (HB1-10, Stellaris) containing 1 µl (125 nM) of probe per sample at 37°C. The cells were washed with Wash Buffer A (Stellaris) and FACS buffer. To visualize the nuclei, the cells were counterstained with Hoechst 33342 (10 µg/ml; Thermo Fisher Scientific) in PBS and incubated for 10 min at room temperature in the dark. Samples were measured on an LSRFortessa (BD Biosciences) or an Amnis ImageStream X MkII cytometer (Accela). The 48 Quasar670-labeled oligonucleotide probes are listed in table S1 and were designed with the Probe Designer tool of Stellaris: www.biosearchtech.com/stellaris-designer.

Imaging flow cytometry and data analysis

CD8⁺ T cells were analyzed in the IDEAS software. The Spot Count mask Dilate [Peak(M11,47S rRNA,Bright,15),1] was applied to count 47S rRNA spots per cell. In addition, the area of the cell, the nucleus, and the nucleolus was measured by applying the masks "Adaptive-Erode(M01,BF1,95)," "AdaptiveErode(M07,DAPI,80)," and "AdaptiveErode [Spot(M11,47S rRNA,Bright, 100,1,2),47S rRNA,90]," respectively. The volume of the cell, the nucleus, and the cytoplasm was calculated in IDEAS by applying the formulas "4/3 × π × [diameter_AdaptiveErode(M01,BF1,95/2)] × [diameter_AdaptiveErode (M01,BF1,95/2)] × [diameter_AdaptiveErode (M01,BF1,95/2)] × [diameter_AdaptiveErode (M07,DAPI,80/2)] × [diameter_AdaptiveErode (M07,DAPI,80/2)] × [diameter_AdaptiveErode (M07,DAPI,80/2)]," and "volume cell – volume nucleus," respectively. The data files were then exported as fcs files and further analyzed with FlowJo v. 10.

Phosphorylated proteins

For intracellular staining, T cells were stained for cell surface markers and fixed with 4% paraformaldehyde. For pS6, cells were permeabilized in Perm Buffer III (BD Biosciences), washed twice, and stained with anti-pS6–specific antibodies (pSer $^{235/6}$: clone 2F9 or D57.2.2E; pSer $^{240/4}$: clone D68F8; all Cell Signaling Technology) at 1:100 in 50 μ l of FACS buffer for 20 min at room temperature. For the H3-pSer 28 stainings, cells were washed after permeabilization in PBS/3% fetal bovine serum, and the H3-pSer 28 antibody was added (1:10) in PBS/3% fetal bovine serum. Cells were incubated for 2 hours at room temperature. Cells were washed twice and stained with Hoechst 33342 before analysis.

EdU labeling

For EdU pulse/chase experiments, 10 µM EdU was added to the culture on day 2 and incubated for 1 hour. Then, cells were washed in medium, and samples were taken after indicated time points. The cells were first stained with antibodies for cell surface markers and fixable viability dye for 20 min at 4°C, fixed with 4% paraformaldehyde for 10 min at room temperature, and permeabilized using Perm Buffer III (BD Biosciences) for 5 min at room temperature in the dark. To detect the amount of incorporated EdU, a reaction mix containing PBS, CuSO₄, fluorescent dye azide, and reaction buffer additive from the Click-iT EdU Alexa Fluor 488 Flow Cytometry Assay Kit (C10420, Thermo Fisher Scientific) was prepared, and 500 μl was added per sample and incubated for 30 min. The cells were washed twice with FACS buffer, stained with Hoechst 33342 (10 µg/ ml) in PBS, and incubated for 10 min at room temperature in the dark. Samples were measured on an LSRFortessa cytometer (BD Biosciences).

HPG incorporation

De novo protein synthesis was measured with the Click-iT HPG Alexa Fluor 488 Kit (C10428, Thermo Fisher Scientific). On day 2 of the stimulation, the cells were washed twice and recultured in methionine-free RPMI 1640 culture medium (A1451701, Thermo Fisher Scientific). HPG was added at 50 μ M and incubated for

1 hour. Then, the samples were harvested and stained with antibodies for cell surface markers and fixable viability dye, fixed with 4% paraformaldehyde, and permeabilized using Perm Buffer III (BD Biosciences). To detect the amount of incorporated HPG, a reaction mix containing PBS, CuSO₄, fluorescent dye azide, and reaction buffer additive from the Click-iT HPG Alexa Fluor 488 Kit was prepared, and 500 μ l was added per sample and incubated for 30 min at room temperature. The cells were washed twice with FACS buffer and subsequently stained with Hoechst 33342 (10 μ g/ml; Thermo Fisher Scientific) in PBS for 10 min at room temperature in the dark. Samples were measured on an LSRFortessa cytometer (BD Biosciences).

Western blotting

Samples were mixed with 1× Laemmli buffer and denatured for 5 min at 95°C. If not indicated otherwise, 5 µg of protein samples was loaded onto an SDS-polyacrylamide gel electrophoresis and run for 15 min at 80 V until samples entered the separation gel and then at 120 V for 1 to 2 hours, depending on protein size. The proteins were blotted on a polyvinylidene difluoride membrane overnight. The membrane was blocked with 5% BSA in tris-buffered saline with Tween 20 (TBS-T) for 1 to 2 hours. Primary antibodies used were specific for mTOR (catalog no. 2983, RRID: AB_2105622), Raptor (2280, AB_561245), Rictor (2114, AB_2179963), S6 (2217, AB_331355), S6K (2708, AB_390722), pS6K-Thr³⁸⁹ (9234, AB_2269803), pS6-Ser^{235/6} (2211, AB_331679), pS6-Ser^{240/4} (4838, AB_659977), and α-tubulin (2125, AB 2619646; all rabbit antibodies, Cell Signaling Technology) at 1:1000 dilutions. Primary antibodies incubated overnight at 4°C with agitation. The antibody for α -tubulin was used as a Ctrl at 1:2000 in TBS-T/5% BSA. The membrane was washed three times for 5 min each with TBS-T. A secondary goat anti-rabbit horseradish peroxidase-linked antibody (7074, AB_2099233, Cell Signaling Technology) was added at 1:1000 in TBS-T/5% BSA and incubated for 1 hour. For detection, 1 ml of enhanced chemiluminescence solution [1 M tris (pH 8.8), 0.2 mM *p*-coumaric acid (Sigma-Aldrich), and 1.25 mM luminol (Fluka)] was mixed with 3 µl of 3% H₂O₂ and pipetted over the membrane for around 1 min. The membrane was then sealed, and an iBright FL1500 (Invitrogen) screen or an x-ray film (Fig. S1) was exposed for 2 s (α -tubulin) to 300 s (other proteins).

Cell preparation and RNA sequencing

Cell sorting of FVD-MFGE8-CD4+ and CD8+ subpopulations of WT and Raptor^{CD4} mice was performed on a FACSAriaIII with a 70-µm-diameter nozzle at the Core Facility for Flow Cytometry of the Biomedical Center (LMU Munich). Sorted cells were resuspended in 250 µl of PBS and 750 µl of TRIzol-LS and stored at -80°C. The prepared samples were delivered to Vertis Biotechnologie AG (Freising, Germany) for RNA sequencing. RNA was isolated and purified using RNeasy columns (74104, QIAGEN), including deoxyribonuclease treatment. RNA preparations were examined by capillary electrophoresis using a MultiNA microchip electrophoresis system (Shimadzu) and a Qubit fluorometer (Thermo Fisher Scientific) to determine 18/28S RNA and total RNA amounts, respectively. RNA samples were first fragmented using ultrasound (four pulses of 30 s each at 4°C). Then, an oligonucleotide adapter was ligated to the 3' end of the RNA molecules. First-strand cDNA synthesis was performed using Moloney murine leukemia virus (M-MLV) reverse transcriptase and the 3' adapter as primer. The first-strand cDNA was purified, and the 5' Illumina TruSeq sequencing adapter was ligated to the 3'

end of the antisense cDNA. The resulting cDNA was polymerase chain reaction—amplified to about 10 to 20 ng/µl using a high-fidelity DNA Pol. The cDNA was purified using the Agencourt AMPure XP kit (Beckman Coulter Genomics) and was analyzed by capillary electrophoresis. The cDNA pool was sequenced on an Illumina NextSeq 500 system using 75–base pair read length.

RNA sequencing data analysis

A fixed number (40×10^6) of sequencing reads per sample was mapped to either the 47S (12.8 kb) rRNA or the entire 45.3-kb rDNA repeat (GenBank accession BK000964.3) using bowtie2 (version 2.2.9) with default parameters. Coverage was calculated using the samtools (version 1.8) depth function. In addition, reads were aligned to the mouse reference genome (version GRCm38) with STAR (version 2.6.0a) to obtain read counts per annotated mouse gene (Ensembl annotation version 92). Gene biotype class assignments were based on the respective Ensembl annotation. Differential expression was tested with DEseq2 (version 1.20.0) with a 10% false discovery rate cutoff to classify significant expression differences. Gene ontology (GO) enrichment analysis was performed using topGO (version 2.32.0) with an expression level–adjusted background set.

Supplementary Materials

The PDF file includes:

Figs. S1 to S4 Table S1

Other Supplementary Material for this manuscript includes the following: MDAR Reproducibility Checklist

REFERENCES AND NOTES

- L. Labanieh, C. L. Mackall, CAR immune cells: Design principles, resistance and the next generation. *Nature* 614, 635–648 (2023).
- A. G. Soerens, M. Künzli, C. F. Quarnstrom, M. C. Scott, L. Swanson, J. J. Locquiao, H. E. Ghoneim, D. Zehn, B. Youngblood, V. Vezys, D. Masopust, Functional T cells are capable of supernumerary cell division and longevity. *Nature* 614, 762–766 (2023).
- E. S. Huseby, E. Teixeiro, The perception and response of T cells to a changing environment are based on the law of initial value. Sci. Signal. 15, eabj9842 (2022).
- A. E. Moran, K. L. Holzapfel, Y. Xing, N. R. Cunningham, J. S. Maltzman, J. Punt, K. A. Hogquist, T cell receptor signal strength in T_{reg} and iNKT cell development demonstrated by a novel fluorescent reporter mouse. *J. Exp. Med.* 208, 1279–1289 (2011).
- N. J. Singh, G. Wolf, "Antigen receptor signaling" in Paul's Fundamental Immunology, M. F. Flajnik, N. J. Singh, S. M. Holland, Eds. (Lippincott Williams & Wilkins, 2023), pp. 734–773.
- J. Zikherman, R. Parameswaran, A. Weiss, Endogenous antigen tunes the responsiveness of naive B cells but not T cells. Nature 489, 160–164 (2012).
- K. A. Frauwirth, J. L. Riley, M. H. Harris, R. V. Parry, J. C. Rathmell, D. R. Plas, R. L. Elstrom, C. H. June, C. B. Thompson, The CD28 signaling pathway regulates glucose metabolism. *Immunity* 16, 769–777 (2002).
- T. Gaber, Y. Chen, P.-L. Krauß, F. Buttgereit, Metabolism of T lymphocytes in health and disease. Int. Rev. Cell Mol. Biol. 342, 95–148 (2019).
- R. D. Michalek, V. A. Gerriets, S. R. Jacobs, A. N. Macintyre, N. J. MacIver, E. F. Mason, S. A. Sullivan, A. G. Nichols, J. C. Rathmell, Cutting edge: Distinct glycolytic and lipid oxidative metabolic programs are essential for effector and regulatory CD4⁺T cell subsets. *J. Immunol.* 186, 3299–3303 (2011).
- D. R. Myers, B. Wheeler, J. P. Roose, mTOR and other effector kinase signals that impact T cell function and activity. *Immunol. Rev.* 291, 134–153 (2019).
- J. D. Powell, C. H. Patel, I.-H. Sun, "Immunometabolism" in *Paul's Fundamental Immunology*, M. F. Flajnik, N. J. Singh, S. M. Holland, Eds. (Lippincott Williams & Wilkins, 2023), pp. 161–203.
- 12. J. A. Shyer, R. A. Flavell, W. Bailis, Metabolic signaling in T cells. Cell Res. 30, 649–659 (2020).
- R. Wang, C. P. Dillon, L. Z. Shi, S. Milasta, R. Carter, D. Finkelstein, L. L. McCormick, P. Fitzgerald, H. Chi, J. Munger, D. R. Green, The transcription factor Myc controls metabolic reprogramming upon T lymphocyte activation. *Immunity* 35, 871–882 (2011).
- R. I. K. Geltink, R. L. Kyle, E. L. Pearce, Unraveling the complex interplay between T cell metabolism and function. *Annu. Rev. Immunol.* 36, 461–488 (2018).

- R. J. Salmond, mTOR regulation of glycolytic metabolism in T cells. Front. Cell Dev. Biol. 6, 122 (2018).
- K. Araki, A. P. Turner, V. O. Shaffer, S. Gangappa, S. A. Keller, M. F. Bachmann, C. P. Larsen, R. Ahmed, mTOR regulates memory CD8 T-cell differentiation. *Nature* 460, 108–112 (2009)
- M. Borsa, I. Barnstorf, N. S. Baumann, K. Pallmer, A. Yermanos, F. Gräbnitz, N. Barandun, A. Hausmann, I. Sandu, Y. Barral, A. Oxenius, Modulation of asymmetric cell division as a mechanism to boost CD8⁺T cell memory. Sci. Immunol. 4, eaav1730 (2019).
- M. Corrado, E. L. Pearce, Targeting memory T cell metabolism to improve immunity. J. Clin. Invest. 132, e148546 (2022).
- P. J. R. Ebert, J. Cheung, Y. Yang, E. McNamara, R. Hong, M. Moskalenko, S. E. Gould, H. Maecker, B. A. Irving, J. M. Kim, M. Belvin, I. Mellman, MAP kinase inhibition promotes T cell and anti-tumor activity in combination with PD-L1 checkpoint blockade. *Immunity* 44, 609–621 (2016).
- R. D. Leone, J. D. Powell, Metabolism of immune cells in cancer. Nat. Rev. Cancer 20, 516–531 (2020).
- S. Liedmann, X. Liu, C. S. Guy, J. C. Crawford, D. A. Rodriguez, D. Kuzuoğlu-Öztürk, A. Guo, K. C. Verbist, J. Temirov, M. J. Chen, D. Ruggero, H. Zhang, P. G. Thomas, D. R. Green, Localization of a TORC1-elF4F translation complex during CD8⁺ T cell activation drives divergent cell fate. *Mol. Cell* 82, 2401–2414.E9 (2022).
- E. L. Pearce, M. C. Walsh, P. J. Cejas, G. M. Harms, H. Shen, L.-S. Wang, R. G. Jones, Y. Choi, Enhancing CD8 T-cell memory by modulating fatty acid metabolism. *Nature* 460, 103–107 (2009).
- R. R. Rao, Q. Li, K. Odunsi, P. A. Shrikant, The mTOR kinase determines effector versus memory CD8⁺T cell fate by regulating the expression of transcription factors T-bet and eomesodermin. *Immunity* 32, 67–78 (2010).
- A. Taylor, J. A. Harker, K. Chanthong, P. G. Stevenson, E. I. Zuniga, C. E. Rudd, Glycogen synthase kinase 3 inactivation drives T-bet-mediated downregulation of co-receptor PD-1 to enhance CD8⁺ cytolytic T cell responses. *Immunity* 44, 274–286 (2016).
- E. W. Weber, K. R. Parker, E. Sotillo, R. C. Lynn, H. Anbunathan, J. Lattin, Z. Good, J. A. Belk,
 B. Daniel, D. Klysz, M. Malipatlolla, P. Xu, M. Bashti, S. Heitzeneder, L. Labanieh, P. Vandris,
 R. G. Majzner, Y. Qi, K. Sandor, L.-C. Chen, S. Prabhu, A. J. Gentles, T. J. Wandless,
 A. T. Satpathy, H. Y. Chang, C. L. Mackall, Transient rest restores functionality in exhausted
 CAR-T cells through epigenetic remodeling. Science 372, eaba1786 (2021).
- G. Y. Liu, D. M. Sabatini, mTOR at the nexus of nutrition, growth, ageing and disease. Nat. Rev. Mol. Cell Biol. 21, 183–203 (2020).
- D. K. Finlay, E. Rosenzweig, L. V. Sinclair, C. Feijoo-Carnero, J. L. Hukelmann, J. Rolf, A. A. Panteleyev, K. Okkenhaug, D. A. Cantrell, PDK1 regulation of mTOR and hypoxia-inducible factor 1 integrate metabolism and migration of CD8⁺T cells. *J. Exp. Med.* 209, 2441–2453 (2012).
- A. J. M. Howden, J. L. Hukelmann, A. Brenes, L. Spinelli, L. V. Sinclair, A. I. Lamond, D. A. Cantrell, Quantitative analysis of T cell proteomes and environmental sensors during T cell differentiation. *Nat. Immunol.* 20, 1542–1554 (2019).
- H. Huang, L. Long, P. Zhou, N. M. Chapman, H. Chi, mTOR signaling at the crossroads of environmental signals and T-cell fate decisions. *Immunol. Rev.* 295, 15–38 (2020).
- J. L. Hukelmann, K. E. Anderson, L. V. Sinclair, K. M. Grzes, A. B. Murillo, P. T. Hawkins, L. R. Stephens, A. I. Lamond, D. A. Cantrell, The cytotoxic T cell proteome and its shaping by the kinase mTOR. *Nat. Immunol.* 17, 104–112 (2016).
- L. V. Sinclair, J. Rolf, E. Emslie, Y.-B. Shi, P. M. Taylor, D. A. Cantrell, Control of amino-acid transport by antigen receptors coordinates the metabolic reprogramming essential for T cell differentiation. *Nat. Immunol.* 14, 500–508 (2013).
- K. Yang, S. Shrestha, H. Zeng, P. W. Karmaus, G. Neale, P. Vogel, D. A. Guertin, R. F. Lamb, H. Chi, T cell exit from quiescence and differentiation into Th2 cells depend on Raptor-mTORC1-mediated metabolic reprogramming. *Immunity* 39, 1043–1056 (2013).
- Z. Cui, G. Napolitano, M. E. G. de Araujo, A. Esposito, J. Monfregola, L. A. Huber, A. Ballabio, J. H. Hurley, Structure of the lysosomal mTORC1-TFEB-Rag-Ragulator megacomplex. *Nature* 614, 572–579 (2023).
- J. A. Martina, Y. Chen, M. Gucek, R. Puertollano, MTORC1 functions as a transcriptional regulator of autophagy by preventing nuclear transport of TFEB. Autophagy 8, 903–914 (2012).
- Y. Wang, Q. Tian, Y. Hao, W. Yao, J. Lu, C. Chen, X. Chen, Y. Lin, Q. Huang, L. Xu, J. Hu, S. Lei, Z. Wei, Y. Luo, Z. Li, L. Hu, J. Tang, Q. Wu, X. Zhou, Y. Wu, Z. Yin, J. Xu, L. Ye, The kinase complex mTORC2 promotes the longevity of virus-specific memory CD4⁺T cells by preventing ferroptosis. *Nat. Immunol.* 23, 303–317 (2022).
- L. Zhang, B. O. Tschumi, I. C. Lopez-Mejia, S. G. Oberle, M. Meyer, G. Samson, M. A. Rüegg, M. N. Hall, L. Fajas, D. Zehn, J.-P. Mach, A. Donda, P. Romero, Mammalian target of rapamycin complex 2 controls CD8 T Cell memory differentiation in a Foxo1-dependent manner. Cell Rep. 14, 1206–1217 (2016).
- A.T. Waickman, J. D. Powell, Mammalian target of rapamycin integrates diverse inputs to guide the outcome of antigen recognition in T cells. J. Immunol. 188, 4721–4729 (2012).
- Q. Zhao, L. W. Duck, F. Huang, K. L. Alexander, C. L. Maynard, P. J. Mannon, C. O. Elson, CD4⁺T cell activation and concomitant mTOR metabolic inhibition can ablate microbiota-specific memory cells and prevent colitis. *Sci. Immunol.* 5, eac6373 (2020).

- M. H. Do, X. Wang, X. Zhang, C. Chou, B. G. Nixon, K. J. Capistrano, M. Peng, A. Efeyan, D. M. Sabatini, M. O. Li, Nutrient mTORC1 signaling underpins regulatory T cell control of immune tolerance. *J. Exp. Med.* 217, e20190848 (2020).
- L. So, K. Obata-Ninomiya, A. Hu, V. S. Muir, A. Takamori, J. Song, J. H. Buckner, R. Savan, S. F. Ziegler, Regulatory T cells suppress CD4⁺ effector T cell activation by controlling protein synthesis. *J. Exp. Med.* 220, e20221676 (2023).
- J. C. Vahl, C. Drees, K. Heger, S. Heink, J. C. Fischer, J. Nedjic, N. Ohkura, H. Morikawa, H. Poeck, S. Schallenberg, D. Rieß, M. Y. Hein, T. Buch, B. Polic, A. Schönle, R. Zeiser, A. Schmitt-Gräff, K. Kretschmer, L. Klein, T. Korn, S. Sakaguchi, M. Schmidt-Supprian, Continuous T cell receptor signals maintain a functional regulatory T cell pool. *Immunity* 41, 722–736 (2014).
- 42. H. Zeng, K. Yang, C. Cloer, G. Neale, P. Vogel, H. Chi, mTORC1 couples immune signals and metabolic programming to establish T_{reg}-cell function. *Nature* **499**, 485–490 (2013).
- D. R. Heintzman, E. L. Fisher, J. C. Rathmell, Microenvironmental influences on T cell immunity in cancer and inflammation. Cell. Mol. Immunol. 19, 316–326 (2022).
- V. Kalia, Y. Yuzefpolskiy, A. Vegaraju, H. Xiao, F. Baumann, S. Jatav, C. Church, M. Prlic,
 A. Jha, P. Nghiem, S. Riddell, S. Sarkar, Metabolic regulation by PD-1 signaling promotes long-lived quiescent CD8 T cell memory in mice. Sci. Transl. Med. 13, eaba6006 (2021).
- A. Trefzer, P. Kadam, S.-H. Wang, S. Pennavaria, B. Lober, B. Akçabozan, J. Kranich, T. Brocker, N. Nakano, M. Irmler, J. Beckers, T. Straub, R. Obst, Dynamic adoption of anergy by antigen-exhausted CD4⁺T cells. *Cell Rep.* 34, 108748 (2021).
- D. Benjamin, M. Colombi, C. Moroni, M. N. Hall, Rapamycin passes the torch: A new generation of mTOR inhibitors. *Nat. Rev. Drug Discov.* 10, 868–880 (2011).
- L. Ye, J. Lee, L. Xu, A.-U.-R. Mohammed, W. Li, J. S. Hale, W. G. Tan, T. Wu, C. W. Davis, R. Ahmed, K. Araki, mTOR promotes antiviral humoral immunity by differentially regulating CD4 helper T cell and B cell responses. J. Virol. 91, e01653–e01616 (2017)
- K. Araki, M. Morita, A. G. Bederman, B. T. Konieczny, H. T. Kissick, N. Sonenberg, R. Ahmed, Translation is actively regulated during the differentiation of CD8⁺ effector T cells. *Nat. Immunol.* 18, 1046–1057 (2017).
- M. Buszczak, R. A. Signer, S. J. Morrison, Cellular differences in protein synthesis regulate tissue homeostasis. Cell 159, 242–251 (2014).
- S. Scheu, D. B. Stetson, R. L. Reinhardt, J. H. Leber, M. Mohrs, R. M. Locksley, Activation of the integrated stress response during T helper cell differentiation. *Nat. Immunol.* 7, 644–651 (2006)
- H. Tan, K. Yang, Y. Li, T. I. Shaw, Y. Wang, D. B. Blanco, X. Wang, J.-H. Cho, H. Wang, S. Rankin, C. Guy, J. Peng, H. Chi, Integrative proteomics and phosphoproteomics profiling reveals dynamic signaling networks and bioenergetics pathways underlying T cell activation. *Immunity* 46, 488–503 (2017).
- T. C. J. Tan, J. Knight, T. Sbarrato, K. Dudek, A. E. Willis, R. Zamoyska, Suboptimal T-cell receptor signaling compromises protein translation, ribosome biogenesis, and proliferation of mouse CD8 T cells. *Proc. Natl. Acad. Sci. U.S.A.* 114, E6117–E6126 (2017).
- D. Shore, B. Albert, Ribosome biogenesis and the cellular energy economy. Curr. Biol. 32, 8611–8617 (2022)
- W. Szaflarski, M. Leśniczak-Staszak, M. Sowiński, S. Ojha, A. Aulas, D. Dave, S. Malla, P. Anderson, P. Ivanov, S. M. Lyons, Early rRNA processing is a stress-dependent regulatory event whose inhibition maintains nucleolar integrity. *Nucleic Acids Res.* 50, 1033–1051 (2022).
- M. Taoka, Y. Nobe, Y. Yamaki, K. Sato, H. Ishikawa, K. Izumikawa, Y. Yamauchi, K. Hirota, H. Nakayama, N. Takahashi, T. Isobe, Landscape of the complete RNA chemical modifications in the human 80S ribosome. *Nucleic Acids Res.* 46, 9289–9298 (2018).
- N. Ban, R. Beckmann, J. H. D. Cate, J. D. Dinman, F. Dragon, S. R. Ellis, D. L. J. Lafontaine, L. Lindahl, A. Liljas, J. M. Lipton, M. A. McAlear, P. B. Moore, H. F. Noller, J. Ortega, V. G. Panse, V. Ramakrishnan, C. M. T. Spahn, T. A. Steitz, M. Tchorzewski, D. Tollervey, A. J. Warren, J. R. Williamson, D. Wilson, A. Yonath, M. Yusupov, A new system for naming ribosomal proteins. *Curr. Opin. Struct. Biol.* 24, 165–169 (2014).
- 57. J. Baßler, E. Hurt, Eukaryotic ribosome assembly. *Annu. Rev. Biochem.* **88**, 281–306 (2019).
- A. Németh, I. Grummt, Dynamic regulation of nucleolar architecture. Curr. Opin. Cell Biol. 52, 105–111 (2018).
- C. Ni, M. Buszczak, The homeostatic regulation of ribosome biogenesis. Semin. Cell Dev. Biol. 136, 13–26 (2023).
- V. Iadevaia, R. Liu, C. G. Proud, mTORC1 signaling controls multiple steps in ribosome biogenesis. Semin. Cell Dev. Biol. 36, 113–120 (2014).
- G. M. Delgoffe, T. P. Kole, Y. Zheng, P. E. Zarek, K. L. Matthews, B. Xiao, P. F. Worley,
 S. C. Kozma, J. D. Powell, The mTOR kinase differentially regulates effector and regulatory
 T cell lineage commitment. *Immunity* 30, 832–844 (2009).
- G. M. Delgoffe, K. N. Pollizzi, A. T. Waickman, E. Heikamp, D. J. Meyers, M. R. Horton, B. Xiao, P. F. Worley, J. D. Powell, The kinase mTOR regulates the differentiation of helper T cells through the selective activation of signaling by mTORC1 and mTORC2. *Nat. Immunol.* 12, 295–303 (2011).
- L. So, J. Lee, M. Palafox, S. Mallya, C. G. Woxland, M. Arguello, M. L. Truitt, N. Sonenberg,
 D. Ruggero, D. A. Fruman, The 4E-BP-elF4E axis promotes rapamycin-sensitive growth and proliferation in lymphocytes. Sci. Signal. 9, ra57 (2016).

- A. S. Rosenberg, A. Singer, Cellular basis of skin allograft rejection: An in vivo model of immune-mediated tissue destruction. *Annu. Rev. Immunol.* 10, 333–360 (1992).
- 65. R. Obst, The timing of T cell priming and cycling. Front. Immunol. 6, 563 (2015).
- H. Rabenstein, A. C. Behrendt, J. W. Ellwart, R. Naumann, M. Horsch, J. Beckers, R. Obst, Differential kinetics of antigen dependency of CD₄⁺ and CD8⁺T cells. *J. Immunol.* 192, 3507–3517 (2014).
- C. G. Proud, "mTORC1 and cell cycle control" in Structure, Function and Regulation of TOR Complexes from Yeasts to Mammals. Part A, M. N. Hall, F. Tamanoi, Eds., vol. 27 of The Enzymes (Academic Press, 2010), pp. 129–146.
- N. Terada, J. J. Lucas, A. Szepesi, R. A. Franklin, J. Domenico, E. W. Gelfand, Rapamycin blocks cell cycle progression of activated T cells prior to events characteristic of the middle to late G₁ phase of the cycle. *J. Cell. Physiol.* 154, 7–15 (1993).
- S. Fumagalli, M. Pende, S6 kinase 1 at the central node of cell size and ageing. Front. Cell Dev. Biol. 10, 949196 (2022).
- O. Meyuhas, Ribosomal protein S6 phosphorylation: Four decades of research. Int. Rev. Cell Mol. Biol. 320, 41–73 (2015).
- G. C. Preston, L. V. Sinclair, A. Kaskar, J. L. Hukelmann, M. N. Navarro, I. Ferrero, H. R. MacDonald, V. H. Cowling, D. A. Cantrell, Single cell tuning of Myc expression by antigen receptor signal strength and interleukin-2 in T lymphocytes. *EMBO J.* 34, 2008–2024 (2015).
- S. H. Ross, C. Rollings, K. E. Anderson, P. T. Hawkins, L. R. Stephens, D. A. Cantrell, Phosphoproteomic analyses of interleukin 2 signaling reveal integrated JAK kinase-dependent and -independent networks in CD8⁺T cells. *Immunity* 45, 685–700 (2016).
- C. H. Patel, Y. Dong, N. Koleini, X. Wang, B. L. Dunkerly-Eyring, J. Wen, M. J. Ranek, L. M. Bartle, D. B. Henderson, J. Sagert, D. A. Kass, J. D. Powell, TSC2 S1365A mutation potently regulates CD8⁺T cell function and differentiation and improves adoptive cellular cancer therapy. *JCl Insight* 8, e167829 (2023).
- R. J. Salmond, J. Emery, K. Okkenhaug, R. Zamoyska, MAPK, phosphatidylinositol 3-kinase, and mammalian target of rapamycin pathways converge at the level of ribosomal protein S6 phosphorylation to control metabolic signaling in CD8 T cells. *J. Immunol.* 183, 7388–7397 (2009).
- K. S. Hamilton, B. Phong, C. Corey, J. Cheng, B. Gorentla, X. Zhong, S. Shiva, L. P. Kane, T cell receptor-dependent activation of mTOR signaling in T cells is mediated by Carma1 and MALT1, but not Bcl10. Sci. Signal. 7, ra55 (2014).
- H. Y. Lu, B. M. Bauman, S. Arjunaraja, B. Dorjbal, J. D. Milner, A. L. Snow, S. E. Turvey, The CBM-opathies–A rapidly expanding spectrum of human inborn errors of immunity caused by mutations in the CARD11-BCL10-MALT1 complex. Front. Immunol. 9, 2078 (2018).
- T. J. O'Neill, T. Seeholzer, A. Gewies, T. Gehring, F. Giesert, I. Hamp, C. Grass, H. Schmidt, K. Kriegsmann, M. J. Tofaute, K. Demski, T. Poth, M. Rosenbaum, T. Schnalzger, J. Ruland, M. Göttlicher, M. Kriegsmann, R. Naumann, V. Heissmeyer, O. Plettenburg, W. Wurst, D. Krappmann, TRAF6 prevents fatal inflammation by homeostatic suppression of MALT1 protease. Sci. Immunol. 6, eabh2095 (2021).
- J. Ruland, L. Hartjes, CARD-BCL-10-MALT1 signalling in protective and pathological immunity. Nat. Rev. Immunol. 19, 118–134 (2019).
- C. C. Thoreen, S. A. Kang, J. W. Chang, Q. Liu, J. Zhang, Y. Gao, L. J. Reichling, T. Sim,
 D. M. Sabatini, N. S. Gray, An ATP-competitive mammalian target of rapamycin inhibitor reveals rapamycin-resistant functions of mTORC1. *J. Biol. Chem.* 284, 8023–8032 (2009).
- J. L. Gowans, B. M. Gesner, D. D. McGregor, in *Biological Activity of the Leucocyte*, G. E. W. Wolstenholme, M. O'Connor, Eds. (Ciba Foundation Study Group, 1961), vol. 10, pp. 32–44.
- J. L. Gowans, D. D. McGregor, D. M. Cowen, C. E. Ford, Initiation of immune responses by small lymphocytes. *Nature*, 196, 651–655 (1962).
- Z. Darzynkiewicz, G. Juan, E. F. Srour, "Differential staining of DNA and RNA" in Current Protocols in Cytometry (Wiley, 2004), 7.3.1–7.3.16.
- J. Ersching, A. Efeyan, L. Mesin, J. T. Jacobsen, G. Pasqual, B. C. Grabiner,
 D. Dominguez-Sola, D. M. Sabatini, G. D. Victora, Germinal center selection and affinity maturation require dynamic regulation of mTORC1 kinase. *Immunity* 46, 1045–1058.e6 (2017).
- M. Mingueneau, T. Kreslavsky, D. Gray, T. Heng, R. Cruse, J. Ericson, S. Bendall, M. H. Spitzer, G. P. Nolan, K. Kobayashi, H. von Boehmer, D. Mathis, C. Benoist, the Immunological Genome Consortium, The transcriptional landscape of αβT cell differentiation. *Nat. Immunol.* 14, 619–632 (2013).
- H. M. Shapiro, Flow cytometric estimation of DNA and RNA content in intact cells stained with Hoechst 33342 and pyronin Y. Cytometry 2, 143–150 (1981).
- S. Battaglioni, D. Benjamin, M. Walchli, T. Maier, M. N. Hall, mTOR substrate phosphorylation in growth control. Cell 185, 1814–1836 (2022).
- C. Chauvin, V. Koka, A. Nouschi, V. Mieulet, C. Hoareau-Aveilla, A. Dreazen,
 N. Cagnard, W. Carpentier, T. Kiss, O. Meyuhas, M. Pende, Ribosomal protein S6 kinase activity controls the ribosome biogenesis transcriptional program. *Oncogene* 33, 474–483 (2014).

- M. Pende, S. H. Um, V. Mieulet, M. Sticker, V. L. Goss, J. Mestan, M. Mueller, S. Fumagalli, S. C. Kozma, G. Thomas, S6K1^{-/-}/S6K2^{-/-} mice exhibit perinatal lethality and rapamycin-sensitive 5'-terminal oligopyrimidine mRNA translation and reveal a mitogen-activated protein kinase-dependent S6 kinase pathway. Mol. Cell. Biol. 24, 3112–3124 (2004).
- C. Decourt, J. Schaeffer, B. Blot, A. Paccard, B. Excoffier, M. Pende, H. Nawabi, S. Belin, The RSK2-RPS6 axis promotes axonal regeneration in the peripheral and central nervous systems. *PLoS Biol.* 21, e3002044 (2023).
- D. Fomina-Yadlin, S. Kubicek, D. Walpita, V. Dancik, J. Hecksher-Sorensen, J. A. Bittker, T. Sharifnia, A. Shamji, P. A. Clemons, B. K. Wagner, S. L. Schreiber, Small-molecule inducers of insulin expression in pancreatic α-cells. *Proc. Natl. Acad. Sci. U.S.A.* 107, 15099–15104 (2010).
- R. J. Salmond, R. J. Brownlie, O. Meyuhas, R. Zamoyska, Mechanistic target of rapamycin complex 1/S6 kinase 1 signals influence T cell activation independently of ribosomal protein S6 phosphorylation. *J. Immunol.* 195, 4615–4622 (2015).
- C. Y. Lin, J. Lovén, P. B. Rahl, R. M. Paranal, C. B. Burge, J. E. Bradner, T. I. Lee, R. A. Young, Transcriptional amplification in tumor cells with elevated c-Myc. Cell 151, 56–67 (2012).
- 93. M. Percharde, A. Bulut-Karslioglu, M. Ramalho-Santos, Hypertranscription in development, stem cells, and regeneration. *Dev. Cell* **40**, 9–21 (2017).
- P. Grozdanov, O. Georgiev, L. Karagyozov, Complete sequence of the 45-kb mouse ribosomal DNA repeat: Analysis of the intergenic spacer. Genomics 82, 637–643 (2003).
- K. J. Abraham, N. Khosraviani, J. N. Y. Chan, A. Gorthi, A. Samman, D. Y. Zhao, M. Wang, M. Bokros, E. Vidya, L. A. Ostrowski, R. Oshidari, V. Pietrobon, P. S. Patel, A. Algouneh, R. Singhania, Y. Liu, V. T. Yerlici, D. D. De Carvalho, M. Ohh, B. C. Dickson, R. Hakem, J. F. Greenblatt, S. Lee, A. J. R. Bishop, K. Mekhail, Nucleolar RNA polymerase II drives ribosome biogenesis. *Nature* 585, 298–302 (2020).
- M. D. Jacob, T. E. Audas, S. T. Mullineux, S. Lee, Where no RNA polymerase has gone before: Novel functional transcripts derived from the ribosomal intergenic spacer. *Nucleus* 3, 315–319 (2012).
- K. Burger, B. Mühl, T. Harasim, M. Rohrmoser, A. Malamoussi, M. Orban, M. Kellner,
 A. Gruber-Eber, E. Kremmer, M. Hölzel, D. Eick, Chemotherapeutic drugs inhibit ribosome biogenesis at various levels. *J. Biol. Chem.* 285, 12416–12425 (2010).
- S.-T. Mullineux, D. L. J. Lafontaine, Mapping the cleavage sites on mammalian pre-rRNAs: Where do we stand? *Biochimie* 94, 1521–1532 (2012).
- E. W. Mills, R. Green, Ribosomopathies: There's strength in numbers. Science 358, eaan2755 (2017).
- S. Šulić, L. Panić, M. Barkić, M. Merćep, M. Uzelac, S. Volarević, Inactivation of S6 ribosomal protein gene in T lymphocytes activates a p53-dependent checkpoint response. *Genes Dev.* 19, 3070–3082 (2005).
- L. Shan, G. Xu, R.-W. Yao, P.-F. Luan, Y. Huang, P.-H. Zhang, Y.-H. Pan, L. Zhang, X. Gao, Y. Li, S.-M. Cao, S.-X. Gao, Z.-H. Yang, S. Li, L.-Z. Yang, Y. Wang, C. C. L. Wong, L. Yu, J. Li, L. Yang, L.-L. Chen, Nucleolar URB1 ensures 3' ETS rRNA removal to prevent exosome surveillance. *Nature* 615, 526–534 (2023).
- 102. R.-W. Yao, G. Xu, Y. Wang, L. Shan, P.-F. Luan, Y. Wang, M. Wu, L.-Z. Yang, Y.-H. Xing, L. Yang, L.-L. Chen, Nascent pre-rRNA sorting via phase separation drives the assembly of dense fibrillar components in the human nucleolus. *Mol. Cell* 76, 767–783.e11 (2019).
- A. Popov, E. Smirnov, L. Kovacik, O. Raska, G. Hagen, L. Stixova, I. Raška, Duration of the first steps of the human rRNA processing. *Nucleus* 4, 134–141 (2013).
- C. Antony, S. S. George, J. Blum, P. Somers, C. L. Thorsheim, D. J. Wu-Corts, Y. Ai, L. Gao, K. Lv, M. G. Tremblay, T. Moss, K. Tan, J. E. Wilusz, A. R. D. Ganley, M. Pimkin, V. R. Paralkar, Control of ribosomal RNA synthesis by hematopoietic transcription factors. *Mol. Cell* 82, 3826–3839.e9 (2022).
- 105. M. D. Claiborne, S. Sengupta, L. Zhao, M. L. Arwood, I. M. Sun, J. Wen, E. A. Thompson, M. Mitchell-Flack, M. Laiho, J. D. Powell, Persistent CAD activity in memory CD8⁺ T cells supports rRNA synthesis and ribosomal biogenesis required at rechallenge. Sci. Immunol. 7, eabh4271 (2022).
- D. L. J. Lafontaine, J. A. Riback, R. Bascetin, C. P. Brangwynne, The nucleolus as a multiphase liquid condensate. Nat. Rev. Mol. Cell Biol. 22, 165–182 (2021).
- T. Moss, F. Langlois, T. Gagnon-Kugler, V. Stefanovsky, A housekeeper with power of attorney: The rRNA genes in ribosome biogenesis. Cell. Mol. Life Sci. 64, 29–49 (2007).
- 108. T. Pederson, The nucleolus. Cold Spring Harb. Perspect. Biol. 3, a000638 (2011).
- F. Frottin, F. Schueder, S. Tiwary, R. Gupta, R. Korner, T. Schlichthaerle, J. Cox, R. Jungmann,
 F. U. Hartl, M. S. Hipp, The nucleolus functions as a phase-separated protein quality control compartment. *Science* 365, 342–347 (2019).
- A. Tzur, J. K. Moore, P. Jorgensen, H. M. Shapiro, M. W. Kirschner, Optimizing optical flow cytometry for cell volume-based sorting and analysis. *PLOS ONE* 6, e16053 (2011).
- T. Wolf, W. Jin, G. Zoppi, I. A. Vogel, M. Akhmedov, C. K. E. Bleck, T. Beltraminelli,
 J. C. Rieckmann, N. J. Ramirez, M. Benevento, S. Notarbartolo, D. Bumann, F. Meissner,
 B. Grimbacher, M. Mann, A. Lanzavecchia, F. Sallusto, I. Kwee, R. Geiger, Dynamics in protein translation sustaining T cell preparedness. *Nat. Immunol.* 21, 927–937 (2020).
- D. Drygin, A. Lin, J. Bliesath, C. B. Ho, S. E. O'Brien, C. Proffitt, M. Omori, M. Haddach, M. K. Schwaebe, A. Siddiqui-Jain, N. Streiner, J. E. Quin, E. Sanij, M. J. Bywater, R. D. Hannan, D. Ryckman, K. Anderes, W. G. Rice, Targeting RNA polymerase I with an

- oral small molecule CX-5461 inhibits ribosomal RNA synthesis and solid tumor growth. Cancer Res. **71**, 1418–1430 (2011).
- D. A. Schneider, A. Michel, M. L. Sikes, L. Vu, J. A. Dodd, S. Salgia, Y. N. Osheim, A. L. Beyer, M. Nomura, Transcription elongation by RNA polymerase I is linked to efficient rRNA processing and ribosome assembly. *Mol. Cell* 26, 217–229 (2007).
- K. Peltonen, L. Colis, H. Liu, R. Trivedi, M. S. Moubarek, H. M. Moore, B. Bai, M. A. Rudek,
 C. J. Bieberich, M. Laiho, A targeting modality for destruction of RNA polymerase I that possesses anticancer activity. *Cancer Cell* 25, 77–90 (2014).
- J. Gui, T. J. Samuels, K. Z. A. Grobicki, F. K. Teixeira, Simultaneous activation of Tor and suppression of ribosome biogenesis by TRIM-NHL proteins promotes terminal differentiation. *Cell Rep.* 42, 112181 (2023).
- N. Terada, R. A. Franklin, J. J. Lucas, J. Blenis, E. W. Gelfand, Failure of rapamycin to block proliferation once resting cells have entered the cell cycle despite inactivation of p70 S6 kinase. J. Biol. Chem. 268, 12062–12068 (1993).
- C. Geier, A. Perl, Therapeutic mTOR blockade in systemic autoimmunity: Implications for antiviral immunity and extension of lifespan. Autoimmun. Rev. 20, 102984 (2021).
- Z. Darzynkiewicz, V. K. Dokov, M. Pienkowski, Dry mass of lymphocytes during transformation after stimulation by phytohaemagglutinin. *Nature* 214, 1265–1266 (1967).
- M. Delarue, G. P. Brittingham, S. Pfeffer, I. V. Surovtsev, S. Pinglay, K. J. Kennedy, M. Schaffer, J. I. Gutierrez, D. Sang, G. Poterewicz, J. K. Chung, J. M. Plitzko, J. T. Groves, C. Jacobs-Wagner, B. D. Engel, L. J. Holt, mTORC1 controls phase separation and the biophysical properties of the cytoplasm by tuning crowding. *Cell* 174, 338–349.e20 (2018).
- 120. J. A. Claypool, S. L. French, K. Johzuka, K. Eliason, L. Vu, J. A. Dodd, A. L. Beyer, M. Nomura, Tor pathway regulates Rrn3p-dependent recruitment of yeast RNA polymerase I to the promoter but does not participate in alteration of the number of active genes. *Mol. Biol. Cell* 15, 946–956 (2004).
- 121. K. M. Hannan, Y. Brandenburger, A. Jenkins, K. Sharkey, A. Cavanaugh, L. Rothblum, T. Moss, G. Poortinga, G. A. McArthur, R. B. Pearson, R. D. Hannan, mTOR-dependent regulation of ribosomal gene transcription requires S6K1 and is mediated by phosphorylation of the carboxy-terminal activation domain of the nucleolar transcription factor UBF. Mol. Cell. Biol. 23, 8862–8877 (2003).
- M. J. James, J. C. Zomerdijk, Phosphatidylinositol 3-kinase and mTOR signaling pathways regulate RNA polymerase I transcription in response to IGF-1 and nutrients. J. Biol. Chem. 279, 8911–8918 (2004)
- C. Mayer, H. Bierhoff, I. Grummt, The nucleolus as a stress sensor: JNK2 inactivates the transcription factor TIF-IA and down-regulates rRNA synthesis. Genes Dev. 19, 933–941 (2005).
- M. Feric, N. Vaidya, T. S. Harmon, D. M. Mitrea, L. Zhu, T. M. Richardson, R. W. Kriwacki, R. V. Pappu, C. P. Brangwynne, Coexisting liquid phases underlie nucleolar subcompartments. *Cell* 165, 1686–1697 (2016).
- 125. A. Amon, A decade of Cdc14 A personal perspective. FEBS J. 275, 5774–5784 (2008).
- 126. M. A. Mensah, H. Niskanen, A. P. Magalhaes, S. Basu, M. Kircher, H. L. Sczakiel, A. M. V. Reiter, J. Elsner, P. Meinecke, S. Biskup, B. H. Y. Chung, G. Dombrowsky, C. Eckmann-Scholz, M. P. Hitz, A. Hoischen, P. M. Holterhus, W. Hulsemann, K. Kahrizi, V. M. Kalscheuer, A. Kan, M. Krumbiegel, I. Kurth, J. Leubner, A. C. Longardt, J. D. Moritz, H. Najmabadi, K. Skipalova, L. S. Blok, A. Tzschach, E. Wiedersberg, M. Zenker, C. Garcia-Cabau, R. Buschow, X. Salvatella, M. L. Kraushar, S. Mundlos, A. Caliebe, M. Spielmann, D. Horn, D. Hnisz, Aberrant phase separation and nucleolar dysfunction in rare genetic diseases. *Nature* 614, 564–571 (2023).
- J. A. Riback, L. Zhu, M. C. Ferrolino, M. Tolbert, D. M. Mitrea, D. W. Sanders, M. T. Wei, R. W. Kriwacki, C. P. Brangwynne, Composition-dependent thermodynamics of intracellular phase separation. *Nature* 581, 209–214 (2020).
- K. Xu, N. Yin, M. Peng, E. G. Stamatiades, A. Shyu, P. Li, X. Zhang, M. H. Do, Z. Wang,
 K. J. Capistrano, C. Chou, A. G. Levine, A. Y. Rudensky, M. O. Li, Glycolysis fuels
 phosphoinositide 3-kinase signaling to bolster T cell immunity. Science 371, 405–410 (2021).
- R. Obst, H.-M. van Santen, D. Mathis, C. Benoist, Antigen persistence is required throughout the expansion phase of a CD4⁺T cell response. J. Exp. Med. 201, 1555–1565 (2005).
- R. Obst, H. M. van Santen, R. Melamed, A. O. Kamphorst, C. Benoist, D. Mathis, Sustained antigen presentation can promote an immunogenic T cell response, like dendritic cell activation. Proc. Natl. Acad. Sci. U.S.A. 104, 15460–15465 (2007).
- J. Kranich, N. K. Chlis, L. Rausch, A. Latha, M. Schifferer, T. Kurz, A. Foltyn-Arfa Kia, M. Simons, F. J. Theis, T. Brocker, In vivo identification of apoptotic and extracellular vesicle-bound live cells using image-based deep learning. *J. Extracell. Vesicles* 9, 1792683 (2020).

Acknowledgments: We thank P. Kadam and V. Luzak for advice and input; A. Kollar, S. Pentz, and J. Wieland for expert technical assistance; A. Bol, B. Popper, L. Böswald, and colleagues for animal husbandry; F. Thümmler (Vertis Biotechnologie AG, Freising-Weihenstephan, Germany) for sequencing; and M. Pende (Institut Necker Enfants Malades, INSERM U1151, Université de Paris, Prance) for mice. **Funding:** This work was supported by the German Research

SCIENCE SIGNALING | RESEARCH ARTICLE

Council grants CRC1054-B07 and OB 150/7-1 (to R.O.), CRC1054-A04 (to D.K.), and CRC1054-Z02 (to J.K.) and the Deutsche Krebshilfe grant 70115440 (to D.K.). **Author contributions:** T.R., S.P., B.A., and R.O. conceptualized the study. T.R., S.P., B.A., and S.J. performed the experiments. T.R., S.P., B.A., S.J., T.S., J.K., and R.O. analyzed the data. T.J.O. and D.K. contributed the conceptual input and provided the $Malt^{1-\ell}$ mice. T.R. and R.O. wrote the manuscript with input from all authors. R.O. supervised the study. Part of this work was done in fulfillment of the M.S. thesis of S.J. at Tor Vergata University of Rome, Italy. **Competing interests:** The authors declare that they have no competing interests. **Data and materials availability:** The sequencing data have been deposited at NCBI GEO under the accession

number GSE217350. All other data needed to evaluate the conclusions in the paper are present in the paper or the Supplementary Materials.

Submitted 23 May 2023 Resubmitted 10 May 2024 Accepted 30 September 2024 Published 22 October 2024 10.1126/scisignal.adi8753